BIOLOGY OF REPRODUCTION (2013) **88**(2):51, 1–15
Published online before print 19 December 2012.
DOI 10.1095/biolreprod.112.103135

A *Wt1-Dmrt1* Transgene Restores DMRT1 to Sertoli Cells of *Dmrt1*$^{-/-}$ Testes: A Novel Model of DMRT1-Deficient Germ Cells[1]

Valentine A. Agbor,[4] Shixin Tao,[5] Ning Lei,[3,4] and Leslie L. Heckert[2,4]

[4]*Department of Molecular and Integrative Physiology, University of Kansas Medical Center, Kansas City, Kansas*
[5]*Department of Nephrology and Hypertension, University of Kansas Medical Center, Kansas City, Kansas*

ABSTRACT

DMRT1 is an evolutionarily conserved transcriptional factor expressed only in the postnatal testis, where it is produced in Sertoli cells and germ cells. While deletion of *Dmrt1* in mice demonstrated it is required for postnatal testis development and fertility, much is still unknown about its temporal- and cell-specific functions. This study characterized a novel mouse model of DMRT1-deficient germ cells that was generated by breeding *Dmrt1*-null (*Dmrt1*$^{-/-}$) mice with *Wt1-Dmrt1* transgenic (*Dmrt1*$^{+/-;tg}$) mice, which express a rat *Dmrt1* cDNA in gonadal supporting cells by directing it from the Wilms tumor 1 locus in a yeast artificial chromosome transgene. Like *Dmrt1*$^{-/-}$ mice, male *Dmrt1*$^{-/-}$ transgenic mice (*Dmrt1*$^{-/-;tg}$) were infertile, while female mice were fertile. Immunohistochemistry and Western blot analysis showed transgenic DMRT1 expressed in supporting cells of the newborn gonads of both sex and in Sertoli cells of the testis afterbirth. Sertoli cells were evaluated by electron microscopy, revealing that maturation of *Dmrt1*$^{-/-;tg}$ Sertoli cells was incomplete. Morphological analysis of testes from 42-day-old mice showed that, compared to *Dmrt1*$^{-/-}$ mice, *Dmrt1*$^{-/-;tg}$ mice have improved seminiferous tubule structure, with lumens present in many. Immunohistochemistry of the polarity markers ESPIN and NECTIN-2 showed that DMRT1 in Sertoli cells is required for NECTIN-2 expression and influences organization of ectoplasmic specializations. Further functional analyses of the transgene on a *Dmrt1*$^{-/-}$ background showed that it did not rescue the decrease in *Dmrt1*$^{-/-}$ testis size, but when expressed on a wild-type background, exogenous DMRT1 prevented the normal age-related decline in testis size and enhanced sperm progressive motility. The studies suggest that DMRT1 in Sertoli cells regulates tubule morphology, spermatogenesis, and sperm function via its effects on Sertoli cell maturation and polarity. Furthermore, expression and function of transgenic DMRT1 in Sertoli cells establishes a novel mouse model of DMRT1-deficient germ cells generated by breeding *Dmrt1*-null mice with *Wt1-Dmrt1* transgenic mice (rescue; *Dmrt1*$^{-/-;tg}$).

DMRT1, male infertility, Sertoli cells, spermatogenesis, testis

INTRODUCTION

Dmrt1 encodes doublesex and mab-3-related transcription factor 1 (DMRT1), a required regulator of testis differentiation and spermatogenesis that shares homology with *Drosophila melanogaster* doublesex and *Caenorhabditis elegans* mab-3 through its DM domain, a highly conserved, cysteine-rich DNA-binding motif featured in proteins involved in sex determination and differentiation [1–19]. In vertebrates, DMRT1 expression is gonad specific and favors the testis in a manner that depends on the species and developmental stage, reflecting its diverse roles in sexual development [1–3, 15, 20–26]. In mammals, just prior to birth, DMRT1 expression becomes testis specific, where it is restricted to undifferentiated spermatogonia and Sertoli cells (SCs) [2, 3, 20, 24, 27, 28]. Its dynamic and highly restricted expression profile and similarity to conserved sexual regulators suggested, early on, that DMRT1 played an important role in male reproduction.

In humans, the chromosomal location of *DMRT1* (9p24.3) is associated with a wide spectrum of disorders that suggested that *DMRT1* haploinsufficiency causes defects in testis development, but no direct evidence exists connecting human DMRT1 to testis function [29–36]. However, studies from many other species argue strongly for its importance to human fertility, as they demonstrate extensive evolutionary constraints on DMRT1 and its requirement for male reproduction [1–3, 7, 9–21, 23–26, 28, 37–40]. To date, most of our knowledge on DMRT1 comes from studies in mice, whereby *Dmrt1* deletion revealed its requirement for male fertility and important roles in establishment and maintenance of SC differentiation and germ cell (GC) expansion and development [2, 3, 41, 42]. The predominant phenotype of *Dmrt1*$^{-/-}$ mice was postnatal male infertility, associated with significantly hypoplastic testes [20, 24]. In contrast, fertility was normal in *Dmrt1*$^{-/-}$ female mice [24, 41]. Testis morphology in *Dmrt1*$^{-/-}$ mice appeared normal through Postnatal Day 7 (P7), except for the central location of GCs within P2–P5 tubules, which indicated that, unlike their wild-type counterparts, the GCs had not yet migrated to the periphery [2, 20, 24]. Additional studies indicated that DMRT1 in both SCs and GCs contributed to the effects on migration [2]. By P10, GC numbers were significantly decreased, while SC numbers increased, and by P14, GCs were absent and seminiferous tubules filled with abundant immature SCs [20, 24]. Defects in GC proliferation and differentiation were implicated by GC loss and reduced levels of γ-H2AX and P-H3, markers for meiosis and mitosis, respectively [20].

Conditional deletion of *Dmrt1* in SCs demonstrated that DMRT1 acts autonomously to regulate cell maturation and nonautonomously to sustain GCs. In SC-specific *Dmrt1* knockout model (*SCDmrt1KO*, *Dhh-Cre*, *Dmrt1*$^{floxed/-}$), GC morphology, migration, and mitosis appeared normal through P7. However, by P9, GCs had accumulated in a disorganized pattern within the lumen, and by P28, they were absent [2]. SCs also appeared normal through P7 but by P9 were slightly

[1]Supported by NIH grant U54HD055763 and the Marion M. Osborn Reproductive Sciences endowment fund.
[2]Correspondence: Leslie L. Heckert, Department of Molecular and Integrative Physiology, University of Kansas Medical Center, 3901 Rainbow Blvd., Kansas City, KS 66160. E-mail: lheckert@kumc.edu
[3]Current address: Department of Biology, University of Utah, 257 South 1400 East, Salt Lake City, UT 84112.

Received: 30 June 2012.
First decision: 28 July 2012.
Accepted: 13 December 2012.

eISSN: 1529-7268 http://www.biolreprod.org
ISSN: 0006-3363

disorganized and by P14 were noticeably more disorganized. By P28, SCs were positioned throughout the tubule and had an immature phenotype, as indicated by decreased AR and GATA1 expression, two markers of SC maturation. More recent studies indicated that DMRT1 is needed in SCs to maintain male sexual differentiation, as SC-specific *Dmrt1* deletion caused postnatal loss of the male-promoting factor SOX9 and subsequent expression of the female-promoting factor FOXL2, suggesting that DMRT1 loss caused differentiated SCs to reprogram into granulosa cells [42]. The delay between the time of *Dmrt1* deletion, presumably prenatal, and feminization of the postnatal testis suggested that DMRT1's participation in SC differentiation occurs several weeks after birth or that its embryonic effects are not erased until then. On the other hand, cell-specific effects of DMRT1 in GCs indicated that, in males, DMRT1 promotes spermatogonial differentiation by direct regulation of *Sohlh1* and prevents entry into meiosis by repressing *Stra8* expression and retinoid signaling [5]. In the fetal female GCs, DMRT1 directly activated STRA8 expression, and its loss caused improper localization of SYCP3 and γH2AX and reduced primordial follicles in the juvenile ovary despite normal fertility [41].

While conditional deletions of *Dmrt1* in SCs effectively demonstrated its role in SC maturation and GC sustenance, limitations in the approaches used to specifically delete *Dmrt1* from GCs have complicated accurate assessment of its GC-specific roles. In one such approach, poor penetrance and ectopic expression of *Tnap*-directed Cre recombinase resulted in *Dmrt1* retention in a number of GCs and its removal from some SCs [2]. Another approach used an *Ngn3*-Cre transgene, which neither expresses in cells contributing to the first wave of spermatogenesis nor effectively deletes *Dmrt1* from the germ line until a week or so after birth [5, 43, 44]. Thus, the current GC-specific deletion models offer ineffective deletion of *Dmrt1* at early postnatal ages. Consequently, there is limited information on the specific role of DMRT1 in the germ line during early postnatal life, which includes several important developmental events, such as GC migration, initiation of spermatogenesis, and formation of the spermatogonia stem cell niche.

To assess DMRT1 cell-specific functions, a transgenic rescue approach was developed that bypasses problems of inefficient gene deletion incurred by poor expression or penetrance of *Cre* recombinase. A transgenic DMRT1 mouse model was generated using the *Wt1* (Wilms tumor suppressor gene 1) locus in a yeast artificial chromosome (YAC) to express DMRT1 only in supporting cells (pregranulosa and pre-Sertoli) of the gonad. Mice expressing DMRT1 only in SCs (rescue; $Dmrt1^{-/-;tg}$) were then derived by breeding *Wt1-Dmrt1* transgenic mice with *Dmrt1*-null mice, effectively generating a GC-specific knockout. Characterization of the transgene showed it was expressed only in supportive cells of the gonads, beginning from early postnatal stages through adulthood. The transgene positively influenced the development and maturation of SCs, partially rescued the seminiferous tubule morphology, and favorably influenced the organization of ectoplasmic specializations. Finally, the *Wt1-Dmrt1* transgene maintained testis size when expressed on a wild-type background and enhanced sperm progressive motility in aging transgenic mice.

MATERIALS AND METHODS

Generation of Wt1-Dmrt1 *Transgene*

A 620-kb YAC containing at least 100 kb of the mouse Wilms tumor 1 gene (*Wt1*) locus was purchased from Research Genetics (YAC620m*Wt1*, address YAC-90-A1, Whitehead I mouse YAC library). A schematic of YAC620m*Wt1* is shown in Figure 1A (top). *Saccharomyces cerevisiae* yeast strain AB1380 (MATa, ura3-52, trp1, ade2-1, his5, lys2-1, can1-100) was grown in Yeast Peptone Dextrose medium and used to propagate the 620-kb YAC containing the mouse *Wt1* gene. YAC-containing yeasts were grown in selective media lacking uracil and tryptophan to maintain the YAC. Propagation was followed as described elsewhere [45].

The targeting vector (pBKS-*Wt1* 5′-*Dmrt1*-HPRT1-LYS2-*Wt1* 3′), generated using PCR-amplified DNA inserts and standard cloning methodology, is depicted in Figure 1A (middle). The vector contains a rat *Dmrt1* cDNA flanked on its 3′ side by the hypoxanthine phosphoribosyl transferase 1 gene (HPRT1) containing a region of exon 8, exon 9 (contains a polyadenylation site) and intervening sequence, the yeast Lysine 2 gene (LYS2; selectable marker), and 776 base pairs (bp) of *Wt1* extending 3′ from its translational start codon. An 825-bp fragment encompassing sequences 5′ to the *Wt1* translational start codon was placed upstream of the *Dmrt1* cDNA in the targeting vector. Primers used to PCR-amplify components of the targeting vector are shown in Supplemental Table S1 (all Supplemental Data are available online at www.biolreprod.org). HPRT1 and LYS2 inserts were PCR amplified from vectors provided by Dr. Kenneth Peterson and Dr. Alan Godwin, respectively, and are described elsewhere [46, 47]. Accuracy of the targeting vector was confirmed by DNA sequencing.

The pBKS-*Wt1* 5′-*Dmrt1*-HPRT1-LYS2-*Wt1*-3′ was linearized by digestion with Cla I and introduced into YAC 620mWT1-containing yeast (AB1380 strain) by spheroplast transformation [48]. Since AB1380 is auxotrophic for lysine, yeasts containing the targeting vector were selected for by growth in the absence of lysine. Yeast with the targeting vector correctly integrated into YAC 620mWT1 were identified by restriction endonuclease mapping, pulse field gel electrophoresis, and Southern blot analysis as described elsewhere [45, 49, 50]. Homologous recombination between YAC and targeting vector was confirmed by PCR amplification and DNA sequence analysis, using Wt1-355 and Dmrt1.16A primers that spanned the 5′ integration site. The resulting YAC, *Wt1-Dmrt1*, contains an in-frame insertion of the *Dmrt1* cDNA with *Wt1* coding sequences (Fig. 1A, bottom).

Wt1-Dmrt1 *and* $Dmrt1^{+/-;tg}$ *Mice*

Wt1-Dmrt1 YAC DNA was isolated by PFGE, concentrated by two-dimensional gel electrophoresis, released from the gel slice by agarase digestion, and filtered through a 0.22-μm filter as described elsewhere [51, 52]. Transgenic mice were generated through the Transgenic and Gene-Targeting Institutional Facility at the University of Kansas Medical Center, using freshly prepared YAC DNA for pronuclear injection into C57B6/SJL F1 zygotes. Two female founders (nos. 30 and 37) and one male founder (no. 13) were obtained and used to generate lines for the production of transgenic offspring by mating to C57BL/6 mice. *Wt1-Dmrt1* transgenic female mice (lines 30 and 37) were crossed with $Dmrt1^{+/-}$ mice (obtained from Dr. David Zarkower and described elsewhere [24]) to create heterozygous transgenic animals ($Dmrt1^{+/-;tg}$) that were mated to generate *Wt1-Dmrt1* transgenic mice homozygous for the *Dmrt1*-null allele ($Dmrt1^{-/-;tg}$). Lines 30 and 37 were crossbred to generate animals with different numbers of transgenes. Because DMRT1 expression was highest in transgenic line 37 and closely resembled that of endogenous DMRT1, phenotypic studies were derived using this line.

Mice were genotyped using PCR and Southern blot analysis of genomic DNA isolated from mouse tail biopsies, as described elsewhere [45, 49, 50]. Sequences of primers used for genotyping are provided in Supplemental Table S2. Mice positive for the transgene were identified by PCR of genomic DNA, using either Wt1-355 and Dmrt1.16A or TGIF0088 and TGIF0090 primer pairs. *Dmrt1* alleles were identified using primers TGIF0105 and TGIF0106 for detection of the $Dmrt1^{+}$ allele and TGIF0105 and TGIF0107 for detection of the $Dmrt1^{-}$ allele. Southern blot analysis was also used for genotyping and transgene copy number determination. In this case, DNA digested with *EcoRI* was resolved by agarose gel electrophoresis, transferred to nylon membrane, and hybridized with a probe corresponding to 165 bp from exon 5 of *Dmrt1* (generated by PCR using *Dmrt1* exon 5 forward and reverse primer pairs). Embryonic sex was deduced from the presence or absence of *Sry*, identified by PCR amplification of genomic DNA (SRY forward and SRY reverse primers).

Mice were maintained on a 12L:12D cycle and given food and water ad libitum. Mice employed in the studies were of mixed background (primarily 129/SvEv and C57BL/6) and followed typical Mendelian inheritance patterns for all genotypes. Animals were cared for in accordance with National Institutes of Health guidelines and with all experimental procedures approved by the Laboratory Animal Research Committee at the University of Kansas Medical Center.

Analysis of Testis Weights and Sperm Function

Reproductive organs were collected from $Dmrt1^{-/-}$, $Dmrt1^{-/-;tg}$, $Dmrt1^{+/+}$, $Dmrt1^{+/+;tg}$, and $Dmrt1^{+/+;tg+tg}$ mice. Mice were euthanized by CO_2

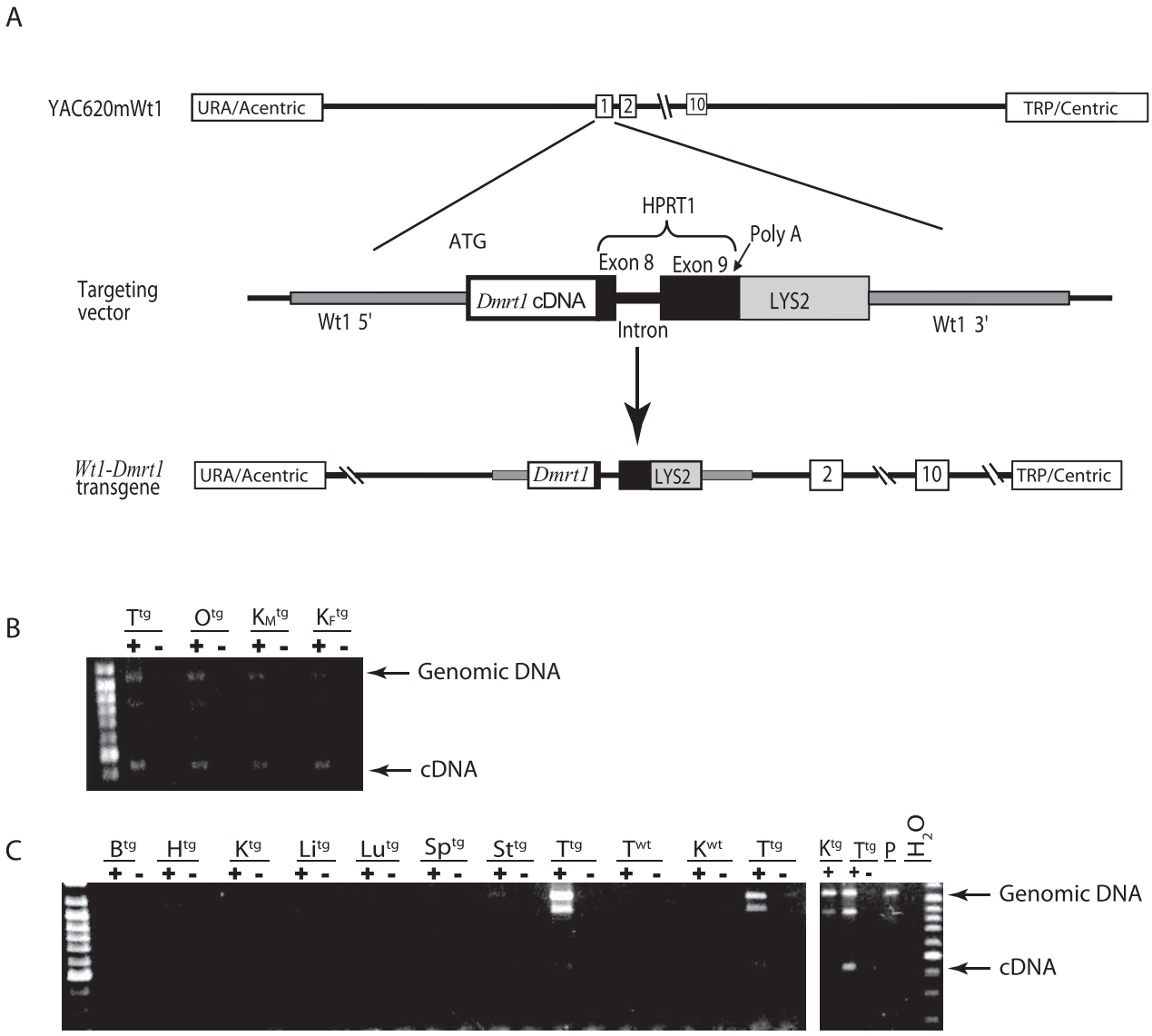

FIG. 1. Generation and tissue-specific expression of the *Wt1-Dmrt1* transgene. **A**) Generation of the *Wt1-Dmrt1* transgene. The rat *Dmrt1* cDNA was inserted in frame with the translational start ATG of mouse Wilms tumor gene 1 (*Wt1*) within the yeast artificial chromosome YAC620mWt1. **Top**: YAC620mWt1; exons = boxed with numbers, URA/Acentric, and TRP/Centric = the pYAC4 acentric vector arms with uracil and tryptophan selectable markers, respectively. **Middle**: targeting vector, pBKS-Wt1-Dmrt1-HPRT1-LTS2. Includes the rat *Dmrt1* cDNA, exons 8 and 9, intron 8 and polyadenylation site of HPRT1, lysine 2 selectable marker (LYS2), 825 bp of *Wt1* sequence 5′ of translational start site (*Wt15′*), and 776 bp of *Wt1* sequence 3′ of translational start site (*Wt13′*). **Bottom**: *Wt1-Dmrt1* transgene after homologous recombination in yeast (AB1380). **B** and **C**) RT-PCR of RNA prepared from different organs from wild-type (wt superscript) and transgenic (tg superscript) mice. **B**) Transgene expression in the kidneys (K) and ovaries (O) and testis (T) of newborn littermates. M and F subscripts indicate male and female, respectively. **C**) Transgene expression in P15 male mice. Tissues are denoted as testis (T), brain (B), heart (H), spleen (Sp), stomach (St), lung (Lu), kidney (K), and liver (Li). The plasmid pBKS-Wt1 5′-Dmrt1-HPRT1-LYS2-Wt1 3′ (P) was included as positive control and water (H_2O) as negative control. cDNA was synthesized in the presence (+) or absence (–) of reverse transcriptase. A ~450-bp band denotes cDNA amplification, while the ~1105-bp band bottom is amplified genomic DNA.

anesthesia followed by cervical dislocation. For each genotype, body and testes weights were determined from at least six male mice, ranging in age from 2 days after birth (P2) to 18 mo. Spermatozoa, obtained from the cauda of 6- and 12-mo *Dmrt1*$^{+/+}$, *Dmrt1*$^{+/+;tg}$, and *Dmrt1*$^{+/+;tg+tg}$ mice epididymis, were collected in Tyrode medium and counted, and approximately 3×10^6 cells were used for assessment of total and progressive motility by computer-assisted semen analysis (CASA), as described elsewhere [53]. Statistical evaluations of changes in testis weight to body/weight ratio (TW/BW), total and progressive motility between groups were done by Student *t*-test ($P < 0.05$).

Histology

One testis from Postnatal Days 7 (P7), 15 (P15), 20 (P20), and 42 (P42) mice were fixed in Bouin solution at room temperature for 4–24 h, depending on size. Testes were rinsed twice with 50% and 70% alcohol, cut in half at the sagittal plane, processed, and embedded in paraffin according to standard procedures. Five-micron sections were cut and mounted on slides, cleared in xylene, rehydrated through graded alcohol series, and stained with periodic acid Schiff reagent and counterstained with hematoxylin. Testis morphology was analyzed using the Nikon Eclipse 80i microscope (Nikon Inc., Instrument Group), and digital images (200× and 400×) were collected using a Retiga 2000R fast camera and QCapture software (QIMAGING).

Immunohistochemistry

Five-micron sections were cleared in xylene, rehydrated through graded alcohol solutions, and heated in 10 mM sodium citrate buffer (pH 6.0) with microwaves (14 min at full power) for antigen retrieval. Sections were blocked using 10% normal goat serum (Zymed Laboratories Inc.) for 60 min at room temperature. For costaining, primary antibody incubations were carried out

overnight at 4°C in blocking solution using the following dilutions: 1:400 of rabbit anti-DMRT1 antibody (custom made for us by Covance Inc.), 1:4 of rat antiserum to GC nuclear antigen 1 (GCNA1, kindly provided by Dr. G. C. Enders), 1:200 of rabbit anti-NECTIN-2 antibody (a gift from Dr. Joseph Tash), 1:200 of rabbit anti-ESPIN antibody (a gift from Dr. T. Rajendra Kumar), 1:100 of goat anti-actin (L19, SC1616), 1:2000 of mouse antiproliferating cell nuclear antigen (PCNA; PC10, SC56, lot no. G1006), 1:100 goat anti-GATA binding protein 4 (GATA4, C20, SC-1237X, lot no. J1090), and 1:100 goat antiandrogen receptor (N-20, SC-816, lot no. J1308). Incubation of the secondary antibody was performed at room temperature for 1 h with a 1:200 dilution of fluorophor-conjugated secondary antibodies (Alexa FluorR 488 goat anti-rabbit IgG; Molecular Probes Inc.), Alexa FluorR 568 donkey anti-rabbit IgG (Molecular Probes), Alexa FluorR 488 donkey anti-goat IgG (Molecular Probes), Cy3-conjugated AffiniPure goat anti-rabbit IgG (Jackson ImmunoResearch Laboratories) and Cy3-conjugated AffiniPure goat anti-rat IgG (Jackson ImmunoResearch Laboratories). Samples were then washed two times in phosphate-buffered saline-Tween20 (PBST; 5 min. each) and DAPI solution (0.8 μg/ml) applied for 10 min to stain nuclei, and slides were washed once and glass cover slides mounted using Fluoromount-G (Southern Biotechnology Associates Inc.). Digital images were collected as above, using fluorescent, DAPI (blue), FITC (green), and TRITC (red) filters. Images were processed using Adobe Photoshop.

Quantification of Germ Cells

The average number of GCs per seminiferous tubule in the testis of P7 mice from *Dmrt1*$^{-/-}$, *Dmrt1*$^{-/-;tg}$, and *Dmrt1*$^{+/+}$ mice were evaluated by counting GCNA1-positive GCs from a minimum of 30 spherical seminiferous tubule from at least three mice for each genotype. The results were analyzed by Student *t*-test to detect significant differences between groups ($P < 0.05$).

Transmission Electron Microscopy

Testes of *Dmrt1*$^{+/+}$, *Dmrt1*$^{-/-}$, and *Dmrt1*$^{-/-;tg}$ P7 and P42 mice were fixed in 2% glutaraldehyde in 0.1 M cacodylate buffer, postfixed in 1% osmium tetroxide/0.8% potassium ferrocyanide, stained in uranyl acetate, and embedded in Epoxy-araldite block. Ultrathin sections (80 nm) were examined at 80 kV using a transmission electron microscope (JEOL 1400EX II; JEOL) for examination of GC and SC morphology. Nuclear cross-sectional area for at least 60 SC nuclei were determined for each group at both time points using Image J analysis software (NIH) as per the request of Image J developers [54]. The results were analyzed by Student *t*-test to detect significant differences between groups ($P < 0.05$).

Western Blot Analysis

Western blot analysis was performed as described elsewhere [27, 55]. Briefly, whole testes extracts from 1-mo-old mice were resolved by SDS-PAGE, transferred to Protran Nitrocellulose membrane (Whatman, GE) and probed overnight at 4°C with a 1:1000 dilution of rabbit anti-DMRT1 (custom made for our laboratory by Covance Inc.) or 1:500 dilution of goat anti-actin (L19, SC1616; Santa Cruz Biotechnology). Following incubation with secondary antibody, donkey anti-goat (1:5000), or donkey anti-rabbit antibody (1:30000) conjugated to HRP (Jackson ImmunoResearch Laboratories), protein complexes were visualized by chemiluminescence.

Western blots were quantitated by densitometry using Image J analysis software (NIH) as per the request of Image J developers [54]. Briefly, each DMRT1 expression band was normalized to its corresponding ACTIN band, and the normalized values were standardized using the values from *Dmrt1*$^{+/+}$ (control) band to obtain relative band densities. For differences between groups, statistical analysis was performed by Student *t*-test ($P < 0.05$).

RT-PCR Analysis of Transgene Expression in Transgenic Mice

F1 offspring were sacrificed and total RNA isolated from various tissues using TRIZOL reagent, according to the manufacturer's procedures (Life Technologies) and tissue-specific transgene expression evaluated by RT-PCR, as described elsewhere [55]. Two microliters of a 20-μl cDNA prep generated from 2 μg RNA were used as template in PCR with primers (listed in Supplemental Table S2) located in the *Dmrt1* cDNA (Dmrt13′) and exon 9 of HPRT1 (HPRT1), which span the HPRT1 intron and allowed differentiation between the expressed transgene and contaminating genomic DNA. Amplified products were examined by agarose gel electrophoresis, with that from the transgene's cDNA, yielding a 434-bp product and that from genomic DNA yielding a 1102-bp product.

Quantitative Real-Time PCR

Real-time reactions were carried out, as described, using a 7900HT Sequence Detection real-time analyzer (Applied Biosystems) [56]. Testis RNA was isolated as above from *Dmrt1*$^{-/-}$, *Dmrt1*$^{-/-;tg}$, and *Dmrt1*$^{+/+}$ P7 mice. First-strand cDNA synthesis was performed using 2 μg RNA with MMLV reverse transcriptase, following manufacturer's instructions (Invitrogen). A 1:10 dilution of cDNA was assayed using a SYBR Green PCR master mix (Applied Biosystems), and primers are listed in Supplemental Table S3. Samples and negative control (water) were run in triplicate. C_t melting curves for endogenous RNA ribosomal L7 (*Rpl7*) was used to calculate ΔC_t values for each sample. *Rpl7* C_t values did not vary across genotype, and the melting curves for *Rpl7* and the genes assayed gave only a single, unique peak for each primer set. $\Delta\Delta C_t$ values were calculated by subtracting the mean P7 wild-type ΔC_t. Fold change was calculated using the $2^{-\Delta\Delta Ct}$ method [57].

RESULTS

Generation of Wt1-Dmrt1 Transgenic Mice

A YAC transgene was generated to exogenously express DMRT1 in SCs and granulosa cells. The transgene was created using a ''knock-in'' strategy that used homologous recombination to insert a targeting vector containing the rat *Dmrt1* cDNA into the mouse *Wt1* locus of YAC620mWt1 (Fig. 1A). The resulting *Wt1-Dmrt1* transgene contains the *Dmrt1* cDNA (beginning with the DMRT1 AUG start codon) inserted in frame with *Wt1*'s start codon in 620mWt1 and, therefore, directs *Dmrt1* expression using *Wt1* regulatory sequences (Fig. 1A bottom). Notably, previous studies showed that YAC620mWt1-derived transgenes expressed only in kidney and gonads, and within the gonads, expression was restricted to supporting cells and initiated prior to sex determination [58, 59]. Three founders were obtained and used to develop transgenic lines 13, 30, and 37, all of which produced pups with the correct chromosomal sex. RT-PCR, using primers that distinguish between rat and mouse *Dmrt1* transcripts and RNA from multiple tissues from newborn and P15 mice, showed transgenic *Dmrt1* expressed only in kidneys and gonads, confirming the expected spatial expression of the transgene (Fig. 1, B and C). Expression was also observed within the ovary from 15.5 days postcoitus (dpc) through P17, but in contrast to an anticipated masculinizing effect of DMRT1, no overt phenotype was noted in female mice (Fig. 1B and Supplemental Figure S1, and data not shown).

Transgenic DMRT1 Is SCSpecific in the Testis

Transgenic male mice were mated with *Dmrt1*$^{-/-}$ female mice, which are fertile, to create *Dmrt1*$^{-/-}$transgenic mice (*Dmrt1*$^{-/-;tg}$) expressing DMRT1 only in SCs. Immunohistochemistry was used to evaluate DMRT1 expression in P7 testes from *Dmrt1*$^{+/+}$, *Dmrt1*$^{-/-}$, and *Dmrt1*$^{-/-;tg}$, and the profiles were compared to confirm proper expression of the transgene (Fig. 2). In *Dmrt1*$^{+/+}$mice (Fig. 2, A–C), DMRT1 immunofluorescence (green) was observed in all SCs and most GCs, as indicated by its overlap with the GC marker GCNA1 (red, yellow in merge). As expected, no DMRT1-positive cells were seen in *Dmrt1*$^{-/-}$ testes (Fig. 2, D–F) or in *Dmrt1*$^{-/-;tg}$ GCs (Fig. 2, G–I), which stained only for GCNA1 (Fig. 2I). Notably, DMRT1 was clearly evident in SCs of *Dmrt1*$^{-/-;tg}$ mouse testes (Fig. 2, G and I). Western blot analysis was also used to evaluate DMRT1 in 1-mo-old testes from mice with different genotypes. DMRT1 and ACTIN levels were quantified by densitometry, and the DMRT1/ACTIN ratio was compared between groups. This indicated that DMRT1 levels in *Dmrt1*$^{-/-;tg}$ testes were slightly higher than that of wild type, while levels in heterozygous and transgenic mice were reduced and elevated, respectively (Fig. 2J). Note, however, that at 1

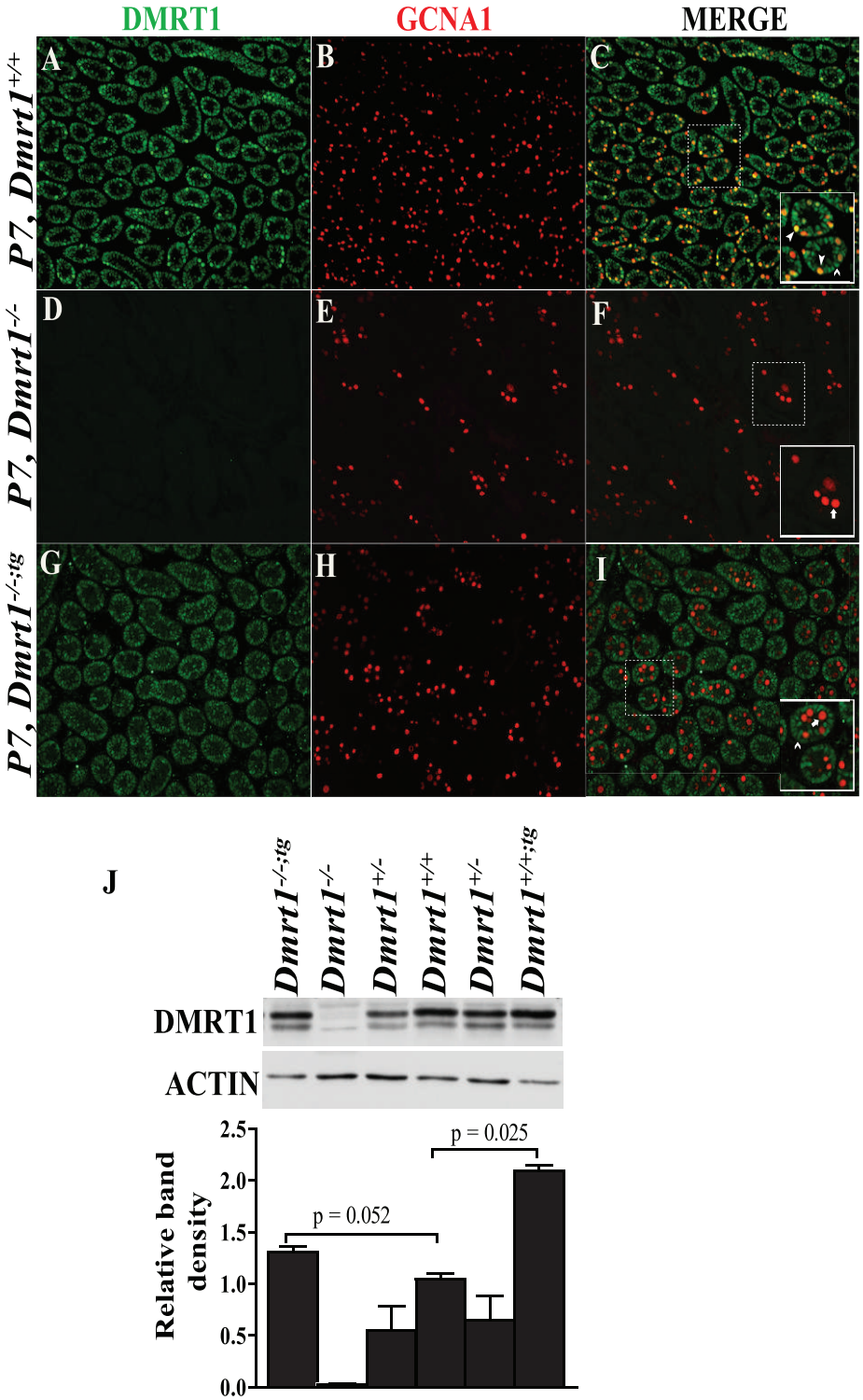

FIG. 2. DMRT1 expression in P7 testes. Coimmunofluorescence of DMRT1 (green) and the GC marker GCNA1 (red) in P7 testes from wild-type (**A**–**C**), *Dmrt1*$^{-/-}$ (**D**–**F**), and *Dmrt1*$^{-/-;tg}$ (**G**–**I**) mice. Individual panels for DMRT1 (**A**, **D**, and **G**) and GCNA1 (**B**, **E**, and **H**) staining and their merged images (**C**, **F**, and **I**) are shown. The solid boxed areas in **C**, **F**, and **I** represent enlarged merged images of areas denoted by the dashed boxes. Within the boxed areas, solid arrowheads denote DMRT1-positive germ cells (yellow), open arrowheads denote DMRT1-positive SCs (green), and arrows denote DMRT1-negative germ cells (red). Note that DMRT1-positive germ cells were observed only in wild-type mice (**C**). Final magnification for all micrographs is ×200. Relative expression levels of DMRT1 in P30 testes from *Dmrt1*$^{+/+}$, *Dmrt1*$^{-/-}$, *Dmrt1*$^{-/-;tg}$, and *Dmrt1*$^{+/+;tg}$ mice (**J**). DMRT1 and ACTIN levels were analyzed by Western blot analysis (top). The bands were quantified by densitometry, and DMRT1 band intensities, relative to that of ACTIN, are represented graphically (bottom). Graphed is the mean DMRT1/ACTIN ratio of three mice/genotype. Error bars represent the SEM.

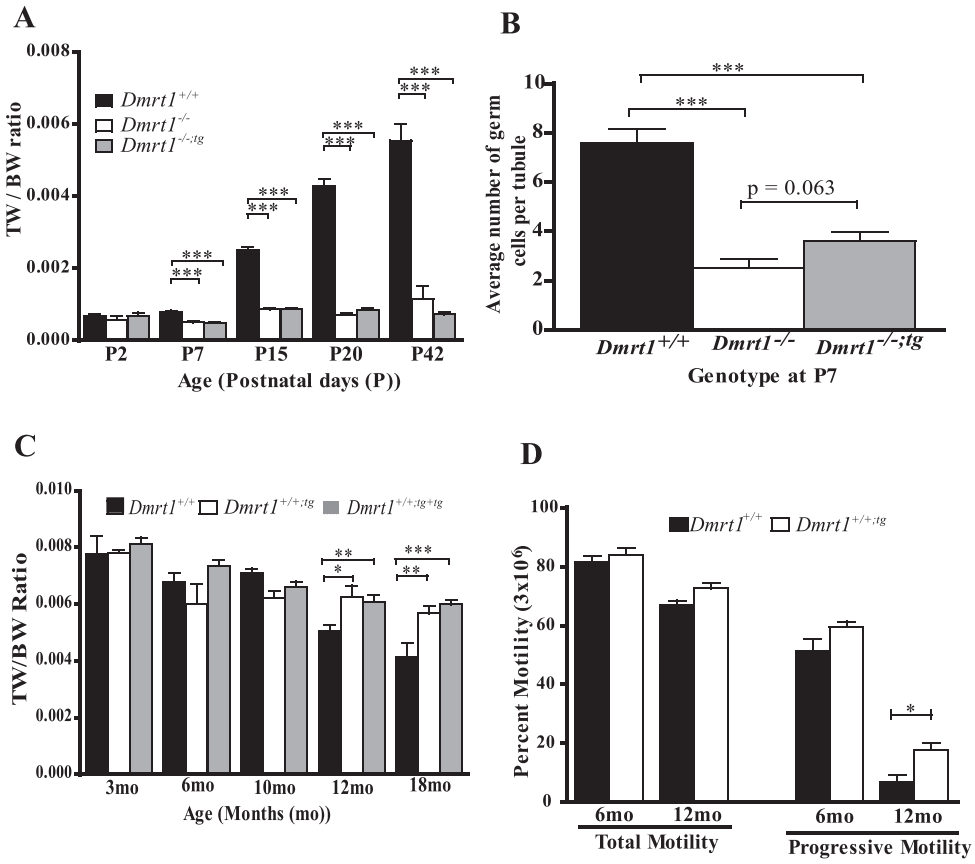

FIG. 3. The *Wt1-Dmrt1* transgene helps maintain testis weights and sperm motility in aging mice. **A**) TW/BW ratios of $Dmrt1^{+/+}$ (black bar), $Dmrt1^{-/-}$ (white bar), and $Dmrt1^{-/-;tg}$ (gray bar) mice at Postnatal Day 2 (P2), 7 (P7), 15 (P15), 20 (P20), and 42 (P42). Graphed is the mean TW/BW + SEM of 3–20 animals. **B**) Average GC number per seminiferous tubule in $Dmrt1^{+/+}$ (black bar), $Dmrt1^{-/-}$ (white bar), and $Dmrt1^{-/-;tg}$ (gray bar) P7 testes. Graphed is the mean number of GCs + SEM from at least 30 tubules/testes in a minimum of three mice per genotype. **C**) Effect of exogenous *Wt1-Dmrt1* transgene on testis weights of wild-type mice. TW/BW ratios for $Dmrt1^{+/+}$ mice (black bar) and $Dmrt1^{+/+}$ mice with one copy ($Dmrt1^{+/+;tg}$; white bar) or two copies of the *Wt1-Dmrt1* transgene ($Dmrt1^{+/+;tg+tg}$; gray bar) at 3, 6, 10, 12, and 18 mo of age. **D**) Total and progressive motility of epididymal sperm from $Dmrt1^{+/+}$ (black bar) and $Dmrt1^{+/+;tg}$ (white bar) mice at 6 and 12 mo of age. Graphed is the mean + SEM of 3–20 animals per genotype. $^{*}P < 0.05$, $^{**}P < 0.001$, and $^{***}P < 0.0001$ (two-tailed Student *t*-test).

mo of age, GCs contribute significantly to the total mass of wild-type testes but not to knockout or rescue testes. Thus, in $Dmrt1^{-/-;tg}$ testes, SCs represent a significantly higher proportion of the total cell mass, and when DMRT1 is measured by Western blot, there is an artificial appearance of elevated DMRT1. However, the levels of DMRT1 in SCs of $Dmrt1^{-/-;tg}$ testes is expected to match that of endogenous SC DMRT1 if adjusted for differences in testis size and higher GC DMRT1 levels.

Transgenic DMRT1 Alleviates the Age-Dependent Decrease in Testis Size and Progressive Sperm Motility

Similar to $Dmrt1^{-/-}$ mice, male $Dmrt1^{-/-;tg}$ mice were infertile, while female mice were fertile. To further evaluate the role of DMRT1 and the effect of the *Wt1-Dmrt1* transgene on fertility, testis size, GC number, and sperm function were measured. Testis size was examined by comparing the TW/BW ratios of $Dmrt1^{+/+}$, $Dmrt1^{-/-}$, and $Dmrt1^{-/-;tg}$ mice at various time points ranging from P2 to P42 (Fig. 3A). At P2, TW/BW ratios were similar for all genotypes. No significant TW/BW change was noted for any genotypes between P2 and P7. However, modest changes for each (increase for $Dmrt1^{+/+}$ and decrease for $Dmrt1^{-/-}$ and $Dmrt1^{-/-;tg}$) were evident when TW/BWs were compared between genotypes, which showed the TW/BW ratios of the $Dmrt1^{-/-}$ and $Dmrt1^{-/-;tg}$ mice were smaller than that of wild type (Fig. 3A). The TW/BW ratio increased in wild-type mice for each time point after P7 (Fig. 3A). In contrast, only a slight increase in TW/BW was noted for $Dmrt1^{-/-}$ and $Dmrt1^{-/-;tg}$ mice between P7 and P15; thereafter, no further change was observed. No significant difference was observed between TW/BW ratios of $Dmrt1^{-/-}$ and $Dmrt1^{-/-;tg}$ mice at any age (Fig. 3A). Therefore, the effect of *Dmrt1* loss on testis size first appears between P2 and P7, and the return of DMRT1 to SCs did not rescue the effect. Since testis weights are strongly associated with GC content, GCNA1 immunofluorescence was used to assess the number of GCs in P7 and P15 testes. The results showed fewer GCNA1-positive cells in P7 testes from $Dmrt1^{-/-}$ and $Dmrt1^{-/-;tg}$ mice compared to wild type, while P15 $Dmrt1^{-/-}$ and $Dmrt1^{-/-;tg}$ testes were devoid of GCs (Supplemental Figure S2). GCNA1-postive GCs from P7 testes were quantified, and the average number per seminiferous tubule was compared between genotypes, confirming that the decreased testis size in the $Dmrt1^{-/-}$ and $Dmrt1^{-/-;tg}$ mice was due to the loss of GCs, which began prior to P7 and was complete by P15 (Fig. 3B).

Since prior studies reported that DMRT1 is needed to maintain SC differentiation, we asked if transgenic DMRT1, when added to SCs of wild-type mice, affected male fertility. To evaluate potential effects of the transgene, the mean body

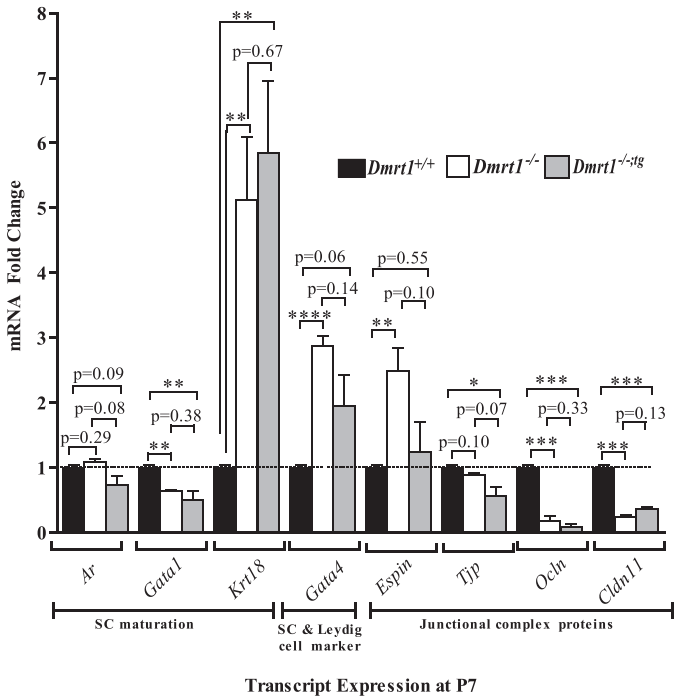

FIG. 4. Expression of genes in response to *Dmrt1* loss. *Espin*, *Ocln*, *Cldn11*, *Tjp*, *Gata1*, *Ar*, and *Krt18* mRNA levels were quantified by quantitative RT-PCR using RNA isolated from testes of *Dmrt1*$^{+/+}$ (black bar), *Dmrt1*$^{-/-}$ (white bar), and *Dmrt1*$^{-/-;tg}$ (gray bar) mice at P7. *$P <$ 0.05, **$P < 0.005$, and ***$P < 0.0005$ (two-tailed Student *t*-test).

(Supplemental Figure S3A) and paired testis (Supplemental Figure S3B) weights were determined for wild-type mice (*Dmrt1*$^{+/+}$) and mice carrying one (*Dmrt1*$^{+/+;tg}$) or two (*Dmrt1*$^{+/+;tg+tg}$) copies of the transgene, at ages ranging from 3 to 18 mo. Each genotype showed age-related increases in body weight, and except for the 6-mo time point, when body weights of the transgenic mice were slightly less than that of wild type, there was no statistical difference between genotypes at any age (Supplemental Figure S3A). For all time points, the mean paired testis weights were also similar between genotypes, except at 18 mo, when testis weights of *Dmrt1*$^{+/+;tg}$ and *Dmrt1*$^{+/+;tg+tg}$ mice were significantly greater ($P < 0.001$) than those of *Dmrt1*$^{+/+}$ mice (Supplemental Figure S3B). In addition, when the paired testes weights were corrected for body weight variation (TW/BW ratio), notable differences were observed between wild-type and the transgenic mice at both 12 and 18 mo. Mice carrying at least one copy of the transgene had significantly higher TW/BW ratios than wild type, but no difference was observed between mice carrying one or two transgenes (Fig. 3C). Note that in wild-type mice, there was a significant age-related decline in both paired testes weights and TW/BW that was absent or less prominent in mice carrying the transgene (Fig. 3C and Supplemental Figure S3B). Therefore, presence of the transgene prevented or slowed the normal age-dependent decline in testis size, suggesting that transgenic DMRT1 preserved SC function and consequently spermatogenic capacity.

To determine if the transgene affected sperm function, CASA was used to measure the total and progressive motility of epididymal sperm isolated from wild-type and transgenic mice. At both 6 and 12 mo, total motility was similar in transgenic and wild-type mice, both showing similar modest reductions in motility (Fig. 3D). In contrast, progressive motility declined significantly between 6 and 12 mo but was less severe for sperm isolated from transgenic mice (Fig. 3D), suggesting that the addition of transgenic DMRT1 to the SCs protected the sperm from the normal functional decline seen in sperm from older animals (Fig. 3D).

DMRT1 Influences SC Maturation

To determine if the transgene rescues defects in SC maturation, quantitative RT-PCR, immunocytochemistry, and SC nuclei ultrastructure analyses were used to compare gene expression, protein, and morphological profiles between *Dmrt1*$^{+/+}$, *Dmrt1*$^{-/-}$, and *Dmrt1*$^{-/-;tg}$ testes; quantitative RT-PCR was used to measure transcript levels for a set of genes, which reflect functional status of the SC, in testes from *Dmrt1*$^{+/+}$, *Dmrt1*$^{-/-}$, and *Dmrt1*$^{-/-;tg}$ P7 mice. P7 mice were used to avoid confounding the data with changes due to GC loss, as is likely with older (~P15) *Dmrt1*$^{-/-}$ and *Dmrt1*$^{-/-;tg}$ mice, which lack GCs. Expression of *Ar*, *Gata1*, and *Krt18* was used to assess SC maturation, with *Ar* and *Gata1* more prominent in mature SCs and *Krt18* a marker of immature cells [60, 61]. The data showed that, while *Ar* mRNA levels were not significantly different between groups, *Gata1* mRNA was reduced ($P < 0.005$) in both *Dmrt1*$^{-/-}$ and *Dmrt1*$^{-/-;tg}$ testes (Fig. 4). Notably, *Krt18* was markedly elevated ($P = 0.0028$) in *Dmrt1*$^{-/-;tg}$ and *Dmrt1*$^{-/-}$ testes (Figure 4). The data are consistent with previous findings that SCs retain an immature phenotype in the absence of *Dmrt1* [24]. Surprisingly, the immature phenotype at P7 was not rescued by the return of DMRT1 to SCs. Additional functional changes were indicated by the increased expression of *Gata4*, which encodes a transcription factor that regulates development and function of fetal and postnatal SCs and Leydig cells [62] in both *Dmrt1*$^{-/-}$ and *Dmrt1*$^{-/-;tg}$ testes (Fig. 4).

Differentiation of SCs coincides with formation of the blood-testis barrier, which contains various membrane and junction-associated inter-Sertoli proteins, such as *OCLN*, *ESPIN*, *CLDN11*, and *TJP1* (*ZO-1*) [63–66]. Transcript levels of the cell junction markers *Ocln*, *Espin*, and *Cldn11* were dramatically changed in *Dmrt1*$^{-/-}$, while more modest changes were noted for *Tjp1* (Fig. 4). Except for *Espin*, significant changes were noted in both *Dmrt1*$^{-/-}$ and *Dmrt1*$^{-/-;tg}$ mice. Of the four cell junction genes, only *Espin* mRNA levels increased in *Dmrt1*$^{-/-}$ testes (~3-fold; $P < 0.03$) or returned to normal when DMRT1 was returned to SCs (Fig. 4). Notably, of the genes investigated, only *Espin* showed significant sensitivity to DMRT1 in SCs, suggesting the other genes were primarily influenced by DMRT1 in GCs.

Immunohistochemistry was used to evaluate AR expression at time points before (P7) and after (P15) SC maturation. Consistent with *Ar* mRNA expression at P7, AR staining was similar in testes from all genotypes at P7, with expression restricted largely to peritubular myoid and Leydig cells (Supplemental Figure S4, A–C). However, by P15, AR expression was notably different in *Dmrt1*$^{-/-}$ and *Dmrt1*$^{-/-;tg}$ compared to wild type (Supplemental Figure S4, D–F). At this time point, AR expression was much more prominent in SCs of wild-type testes than at P7 (compare Supplemental Figure S4, A and D). In contrast, the number of AR-positive SCs was greatly reduced at P15 in *Dmrt1*$^{-/-}$ testes compared to wild type, while in *Dmrt1*$^{-/-;tg}$ the number of positive SCs was intermediated between wild-type and *Dmrt1*$^{-/-}$ (Supplemental Figure S4, D–F).

SC maturation was further assessed using transmission electron microscopy to examine ultrastructure of the nucleus at P7 and P42 (Fig. 5: SC and GC nuclei traced by black and

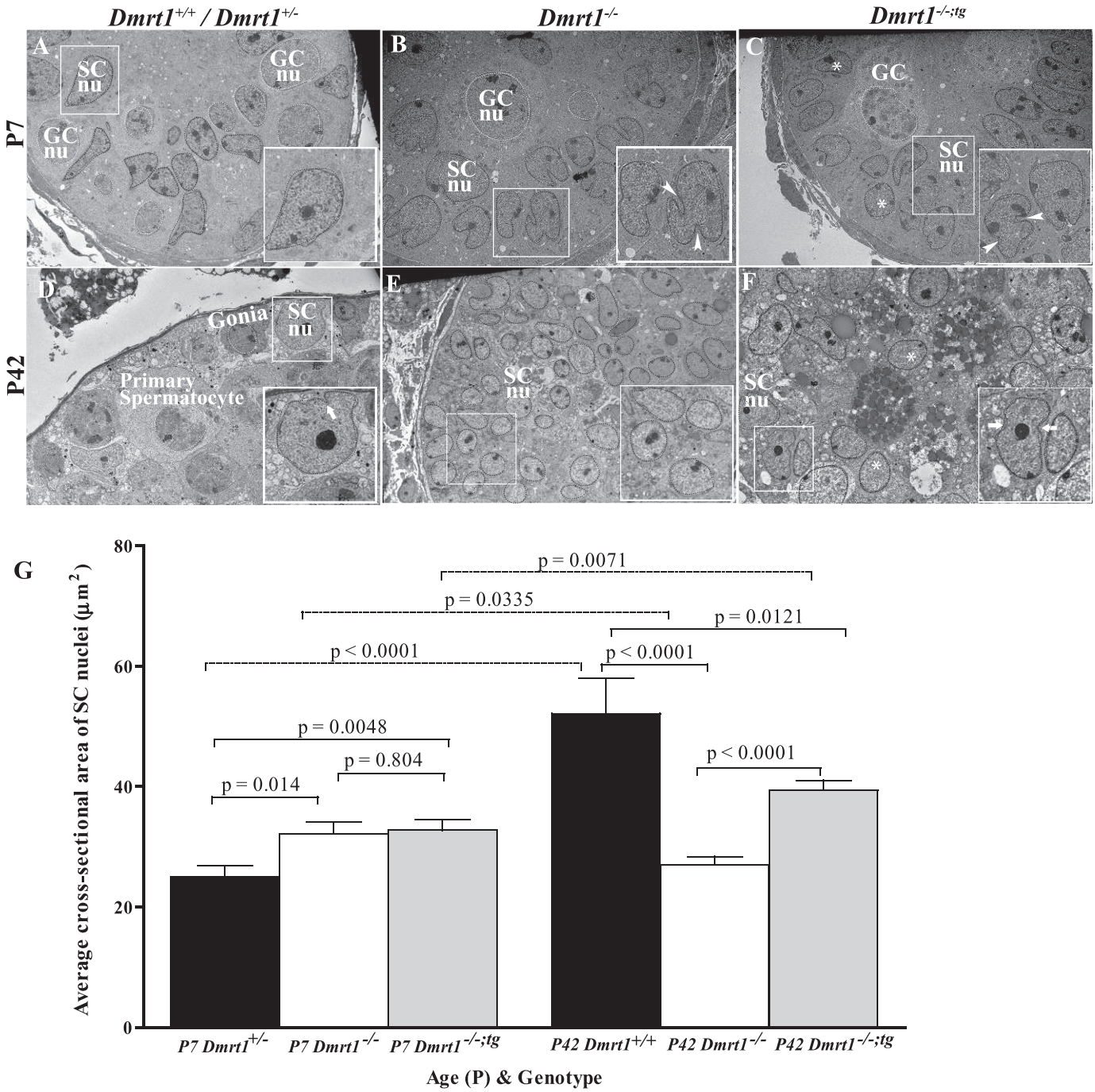

FIG. 5. Electron microscopic evaluation of SC nuclei. Testes from *Dmrt1*$^{+/+}$ or *Dmrt1*$^{+/-}$ (**A** and **D**), *Dmrt1* $^{-/-}$ (**B** and **E**), and *Dmrt1*$^{-/-;tg}$ (**C** and **F**) mice were evaluated at P7 (**A**–**C**) and P42 (**D**–**F**). Some GC (GCnu) and SC nuclei (SCnu) are traced by white and black lines, respectively. **A**–**C**) Electron micrographs of seminiferous tubules from P7 *Dmrt1*$^{+/-}$, *Dmrt1*$^{-/-}$, and *Dmrt1*$^{-/-;tg}$ testes. **A**) *Dmrt1*$^{+/-}$ tubule showing normal ultrastructure of SC nucleus (inset). Magnification ×3040. **B**) *Dmrt1*$^{-/-}$ tubule showing abnormal SC nuclei. Boxed SC nuclei denoted the irregular shaped and multilobulated nuclei containing deep invaginations (arrowheads). Magnification ×3040. **C**) *Dmrt1*$^{-/-;tg}$ tubule showing a mixed population of normal- and abnormal-looking SC nuclei. The normal (asterisk) and abnormal (arrowhead) nuclei shared characteristics with *Dmrt1*$^{+/+}$ and *Dmrt1*$^{-/-}$ mice, respectively. Magnification ×2280. **D**–**F**) Electron micrographs of seminiferous tubules from P42 *Dmrt1*$^{+/+}$, *Dmrt1*$^{-/-}$, and *Dmrt1*$^{-/-;tg}$ testes. **D**) *Dmrt1*$^{+/+}$ tubule showing normal ultrastructure of SC and GCs. Note that SC nuclei are larger with considerable perinuclear cytoplasm and have an irregular ovoid shape with invaginations (arrow) and significant nucleolus. Magnification ×2280. **E**) *Dmrt1*$^{-/-}$ tubule showing SCs with many regular round nuclei (asterisk) and scanty amount of cytoplasm (inset). Note that there are no GCs present. Magnification ×1900. **F**) *Dmrt1*$^{-/-;tg}$ tubule showing many regular shaped, round SC nuclei (asterisk) with a few irregular, indented (arrows) nuclei, and prominent nucleolus. Magnification ×3040. **G**) The average cross-sectional area of SC nuclei in P7 and P42 testes of control (black bars), *Dmrt1*$^{-/-}$ (white bars), and *Dmrt1*$^{-/-;tg}$ (gray bars) testes. Graphed is the mean cross-sectional area of ≥60 nuclei per genotype per time point. Error bars represent the SEM. Statistical significance was determined using a two-tailed Student *t*-test with *P*-values denoted between relevant pairings.

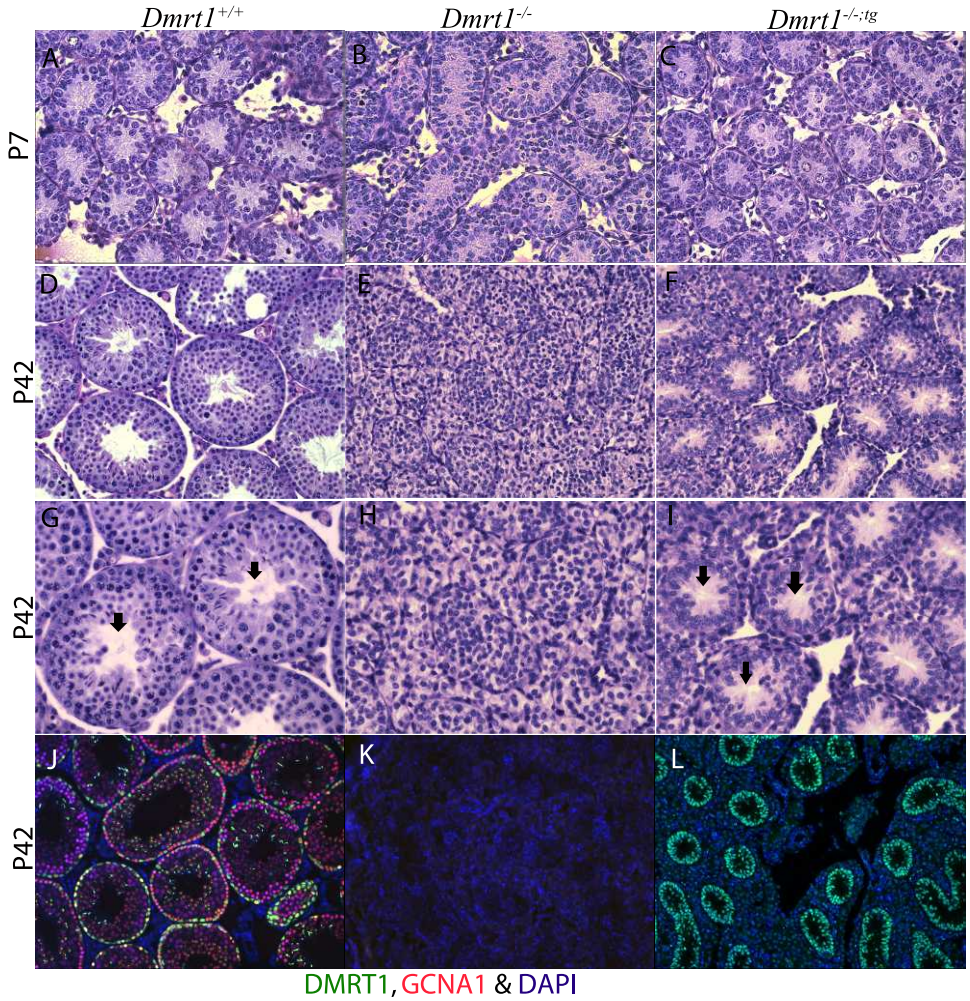

FIG. 6. Morphological analysis of P7 and P42 mouse testes. Periodic acid Schiff staining of P7 (**A**–**C**) and P42 (**D**–**I**) testis section from wild-type (**A**, **D**, and **G**), *Dmrt1*$^{-/-}$ (**B**, **E**, and **H**), and *Dmrt1*$^{-/-;tg}$ (**C**, **F**, and **I**) mice. Note that the addition of the transgene (i.e., in *Dmrt1*$^{-/-;tg}$ mice) partially restored seminiferous tubule morphology. Magnification ×400 (**A**–**F**) and ×600 (**G**–**I**). Arrows (**G** and **I**) denote the presence of defined lumens, which were absent from the *Dmrt1*$^{-/-}$ testis (**H**). Immunohistochemical analysis of wild-type (**J**), *Dmrt1*$^{-/-}$ (**K**), and *Dmrt1*$^{-/-;tg}$ (**L**) at P42 (magnification ×200). Testis sections were evaluated using fluorescently labeled antibodies against DMRT1 (green) and GCNA1 (red) and DAPI for nuclei (blue).

white lines, respectively). At P7, SC nuclei of *Dmrt1*$^{+/-}$ mice had a regular columnar contour without invaginations and were located away from the basement membrane (Fig. 5A, insert). Interestingly, nuclei of P7 *Dmrt1*$^{-/-}$ SCs were more irregular shaped, with multiple invaginations and more prominent areas of condensed chromatin, features associated with mature SCs (Fig. 5B) [67]. In P7 *Dmrt1*$^{-/-;tg}$ mice, some rounded, regular-shaped SC nuclei, similar to that observed in the wild type, were observed (Fig. 5C, asterisks), but the majority appeared like those in P7 *Dmrt1*$^{-/-}$ mice (Fig. 5C, arrowheads in insert). At P42, *Dmrt1*$^{+/+}$ SC nuclei were located closer to the basement membrane, the nucleolus had formed a central granular condensed area, and the nuclear membrane was invaginated (Fig. 5D). P42 *Dmrt1*$^{-/-}$ nuclei were predominantly round, columnar, or ovoid shaped; without invaginations; and not closely associated with the basement membrane of the tubule (Fig. 5E). *Dmrt1*$^{-/-}$ nucleoli were found at the periphery of the nucleus, and the chromatin was arranged in irregular granular clusters. Morphology of SC nuclei in P42 *Dmrt1*$^{-/-;tg}$ mice appeared intermediate to that observed in wild-type and *Dmrt1*$^{-/-}$ mice, comprising a mixture of nuclei that were either regular round or irregular ovoid (compare nuclei in enlarged insert in Figu. 5, E and F). Some nuclei had invaginations (Fig. 5F, arrows in insert) and nucleoli that formed a central granular condensation area (Fig. 5F, insert). However, most ovoid nuclei had nucleoli located at the periphery of the nuclear membrane and chromatin arranged in irregular granular clusters (Fig. 5F, asterisks).

Since SC nuclei increase in area approximately 3-fold between 1 and 5 wk after birth, nuclear cross-sectional areas were quantified in SCs of each genotype as a means to further assess the role of DMRT1 in cell maturation [67, 68]. At P7, the average nuclear cross-sectional area was significantly greater in SCs from *Dmrt1*$^{-/-}$and *Dmrt1*$^{-/-;tg}$ mice than from *Dmrt1*$^{+/-}$ mice but not different between nuclei from *Dmrt1*$^{-/-}$ and *Dmrt1*$^{-/-;tg}$ mice (Fig. 5G). At P42, the average nuclear cross-sectional area of *Dmrt1*$^{+/+}$ SCs was significantly greater than that of *Dmrt1*$^{-/-}$ or *Dmrt1*$^{-/-;tg}$ SCs (Fig. 4G). In addition, the average nuclear area of *Dmrt1*$^{-/-;tg}$ SCs at P42 was significantly greater than that of *Dmrt1*$^{-/-}$ SCs, indicating that the exogenous DMRT1 in *Dmrt1*$^{-/-;tg}$ testes induced a significant increase in the nuclear area of *Dmrt1*$^{-/-}$ SCs. Notably, both control (*Dmrt1*$^{+/-}$ and *Dmrt1*$^{+/+}$) and *Dmrt1*$^{-/-;tg}$ SCs showed significant increases in nuclear area from P7 to P42, while the nuclear area of *Dmrt1*$^{-/-}$ SCs decreased during this time (Fig. 5G). These results are consistent with the morphological

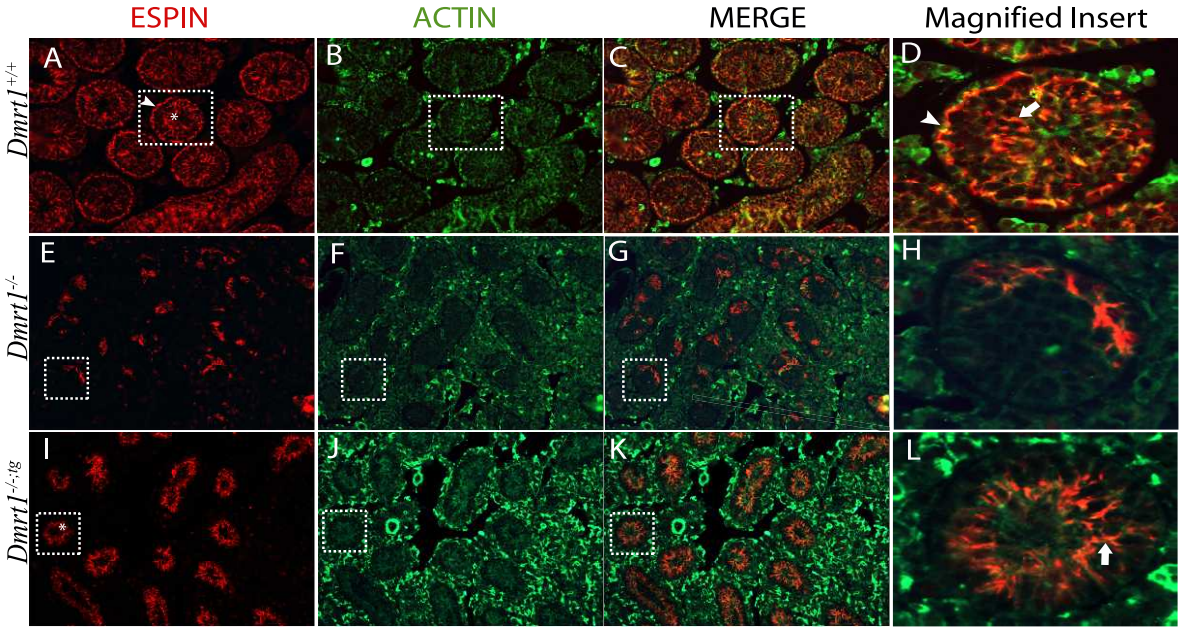

FIG. 7. Immunolocalization of ESPIN and ACTIN in P42 mouse testes. Coimmunofluorescence of ESPIN (red) and ACTIN (green) in testes sections from wild-type (**A**–**D**), *Dmrt1*$^{-/-}$ (**E**–**H**), and *Dmrt1*$^{-/-;tg}$ (**I**–**L**) mice. Shown are individual panels for ESPIN (**A**, **E**, and **I**) and ACTIN (**B**, **F**, and **J**) staining, their merged (**C**, **G**, and **K**) images, and enlarged merged images of areas denoted by boxes (**D**, **H**, and **L**). Arrowhead in **A** and asterisk in **A** and **I** show basal and apical ES, respectively. Arrowhead in **D** and arrow in **D** and **L** show colocalization of ESPIN and ACTIN at the basal and apical ES, respectively. Final magnification of all panels except for magnified inserts was ×200.

assessment, which suggested that, at P7, DMRT1-deficiency leads to a more mature nuclear phenotype, but by P42, the nuclei of *Dmrt1*$^{-/-}$ SCs were characteristically immature, while *Dmrt1*$^{-/-;tg}$ SC nuclei had characteristics intermediate between that of wild type and *Dmrt1*$^{-/-}$. Overall, the data indicate that the return of DMRT1 to SC of *Dmrt1*-null mice positively influenced the maturation and/or development of SCs.

Transgenic DMRT1 Partially Preserves Testis Morphology and Tubule Polarity

Confirming earlier studies, immunohistochemistry of P7 testes demonstrated the requirement for DMRT1 in GC radial migration (Fig. 2, C and F; [2, 20, 24, 69]). Thus, in *Dmrt1*$^{-/-}$ testes, the GCs were confined to the lumen of the seminiferous tubule, while in *Dmrt1*$^{+/+}$testes, they had migrated to the basement membrane. Furthermore, GC migration was also defective in P7 *Dmrt1*$^{-/-;tg}$ testes, indicating that GC migration requires DMRT1 in GCs (Fig. 2). Histological analyses of P7 *Dmrt1*$^{-/-;tg}$, *Dmrt1*$^{-/-}$, and *Dmrt1*$^{+/+}$ testes revealed similar tubule morphology between the genotypes, with only modest differences noted in organization (Fig. 6, A–C). However, by P42, *Dmrt1*$^{-/-}$ testes were severely disorganized compared to wild type, with little evidence of tubule structure. In contrast, *Dmrt1*$^{-/-;tg}$ testes had distinct seminiferous tubule structures, many with obvious lumens and without the accumulated SCs seen in *Dmrt1*$^{-/-}$ testes (Fig. 6, D–K). To confirm the expression of transgenic DMRT1 in adult testes, immunohistochemistry was performed using antibodies for DMRT1 (green) and GCNA1 (red). In P42 wild-type testes, DMRT1 was observed in both SCs and GCs (Fig. 6J, green and yellow stained cells, respectively). Note that the green staining observed on spermatids represents nonspecific binding of the secondary antibody. DMRT1 expression was not evident in P42 *Dmrt1*$^{-/-}$ testes (Fig. 6K), while in *Dmrt1*$^{-/-;tg}$ testes, its expression was clearly maintained at P42, with notable SC staining within well-structured seminiferous tubules (Fig. 6L). In both *Dmrt1*$^{-/-}$ and *Dmrt1*$^{-/-;tg}$ testes, GCNA1 staining was absent, confirming the lack of GCs. The restoration of tubule morphology further demonstrates function of the transgene-derived DMRT1 in SCs. In addition, it confirms that DMRT1 in SCs is needed to maintain seminiferous tubule structure and, together with the gene expression changes, implicates DMRT1 in the organization of the basal and apical compartments.

To evaluate polarity of seminiferous tubules, immunofluorescence was used to detect the expression of ACTIN and two adaptor proteins of the apical and basal ectoplasmic specialization (ES), ESPIN and NECTIN-2, in the adult (P42) testis. In *Dmrt1*$^{+/+}$ testes, ESPIN, an actin-binding/bundling protein, localized together with ACTIN (Fig. 7, A–D) at the basal ES, seen as curvilinear and arching structures at the basal aspect of the seminiferous epithelium (Fig. 7, A and D, arrowhead), and the apical ES, in association with elongating spermatids along columns within the seminiferous epithelium (Fig. 7, A and D, asterisk and arrow). In *Dmrt1*$^{-/-}$ testes, ESPIN staining was significantly reduced and only partially overlapped with that of ACTIN (Fig. 7, E–H). It was also observed in irregular, random patches that lacked the characteristic polarity seen in the wild-type mice. Notably, in *Dmrt1*$^{-/-;tg}$ testes, ESPIN staining was absent from the basal aspect despite the presence of ACTIN and present in the adluminal area, where it colocalized with ACTIN along clearly oriented projections (Fig. 7, I–L). This suggested that DMRT1 in SCs is needed for polarity of the seminiferous tubules and structuring the apical ES. Similar results were also obtained for NECTIN-2 (Fig. 8). NECTIN-2 staining in *Dmrt1*$^{-/-}$ testes was barely detectible and without notable organization (Fig. 8B). As seen in *Dmrt1*$^{-/-;tg}$ testes, addition of DMRT1 to SCs recovered NECTIN-2 expression, which, like ESPIN, localized to projecting structures at the adluminal edge of the tubule (Fig. 8C). The data reveal that DMRT1 in SCs is required for expression of ESPIN and NECTIN-2 and facilitates their localization to the apical compartment, supporting a role in apical ES organization. The data also

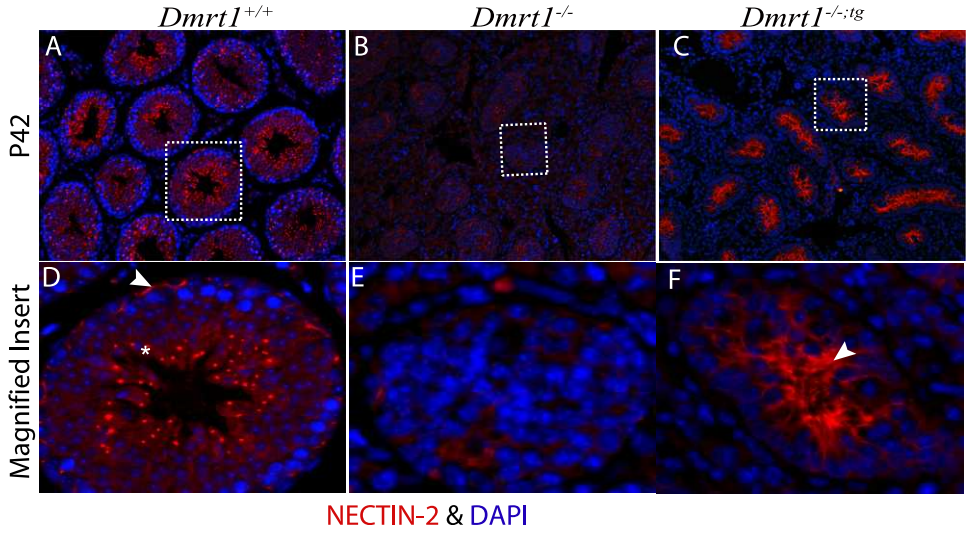

FIG. 8. Immunolocalization of NECTIN-2 in P42 mouse testes. Immunofluorescence of NECTIN-2 (red) and DAPI stain (blue) in testes sections from wild-type (**A**), *Dmrt1*$^{-/-}$ (**B**), and *Dmrt1*$^{-/-;tg}$ (**C**) mice. **D**–**F** show enlarged images of the areas denoted by boxes in **A**–**C**. Arrowhead and asterisk in **D** show basal and apical ES, respectively. Arrowhead in **F** shows ES in the adluminal compartment of the seminiferous tubule. Final magnification of all panels except for magnified inserts was ×200.

indicate that DMRT1 in GCs, either directly or through its effects on GC survival, is required for the localization of NECTIN-2 and ESPIN to the basal ES.

DISCUSSION

The requirement for DMRT1 in establishing male fertility motivated numerous studies to uncover its specific role in spermatogenesis. However, because multiple cell types express DMRT1 and its activity changes with differentiation, a comprehensive understanding of its functions requires strategies that examine its activity separately in SCs and GCs and capture different developmental time points. Several excellent mouse models and temporal studies have contributed to our understanding of DMRT1's function, which is far from complete, particularly with respect to its cell-specific roles, its target genes, and its activities in early postnatal versus adult testes. To facilitate our understanding of DMRT1's specific functions in SCs and GCs, we developed a transgenic mouse model that expresses DMRT1 from the *Wt1* locus within a YAC. Crossing the transgenic mice into the *Dmrt1*$^{-/-}$ background created a unique model in which DMRT1 is expressed only in SCs. Here we report the generation and characterization of this mouse model.

The *Wt1-Dmrt1* transgene used the *Wt1* locus within a YAC to direct DMRT1 specifically to SCs of the testis. Unlike small transgenes, YACs (or BACs) are much less subject to integration site effects, resulting in expression that is often copy number dependent and directed only by sequences in the transgene [70]. Notably, the tissue and cellular profile of transgenic *Dmrt1*/DMRT1 matched the expected pattern of *Wt1* and rescued testis expression profiles of several genes altered in *Dmrt1*$^{-/-}$ testes (Figs. 1, 2, 4, 7, and 8, and data not shown). The data also showed that transgene was expressed in the testis at P0, P7, P15, and P42 and in somatic cells of the ovary at 15.5 dpc (Supplemental Figure S1). Earlier time points were not evaluated because transgenic DMRT1 cannot be distinguished from the endogenous protein, which is present in testis somatic cells from 11.5 onward and in ovarian somatic cells until about 15.5 dpc [27]. However, previous studies using the same YAC showed it was active in somatic cells at 11.5 dpc, suggesting that the *Wt1-Dmrt1* transgene also produces DMRT1 in supporting somatic cells of 11.5 dpc undifferentiated gonads [58]. In addition, immunohistochemistry of *Dmrt1*$^{-/-;tg}$ mice showed that transgenic DMRT1 produced only in SCs of the testis, while Western blot analysis indicated that it is expressed at levels that match the endogenous protein. Together, the findings indicate that transgenic DMRT1 is expressed in SCs from 15.5 dpc through P42 at levels predicted to replicate its activity within SCs. Transgenic *Dmrt1* also followed the kidney expression pattern for *Wt1*. With the exception of one founder animal that died, there was no evidence of kidney pathology. In the postnatal kidney, *Wt1-Dmrt1* mRNA was observed at P0 and P15, but the P15 signal was much lower than that at P0, and additional amplification cycles were required for its detection (Fig. 1, B and C, right). This drop in expression is consistent with previous reports on mouse *Wt1* that showed that kidney expression dropped dramatically by P15 [71]. Overall, the data confirmed that the spatial and temporal expression pattern of *Wt1-Dmrt1* accurately matched that reported previously for both endogenous *Wt1* and the YAC used to make the transgene [58, 72, 73].

Phenotypic analysis of wild-type and *Dmrt1*$^{-/-}$ mice expressing the *Wt1-Dmrt1* transgene was performed to elucidate DMRT1 functions. Although thorough studies were not performed on female mice, no abnormalities were noted in ovarian development or function for any of the investigated genotypes (data not shown). Studies on male mice confirmed past findings and revealed several novel functions. First, evaluation of *Dmrt1*$^{-/-}$ and *Dmrt1*$^{-/-;tg}$ mice both supported and enhanced our understanding of its role in SC differentiation. After puberty, SCs, the specialized testicular somatic cells that support GC development, are considered terminally differentiated, which is signified by their inability to proliferate, the formation of functional inter-SC tight junctions, and the acquisition of specific functions and proteins not present in immature SCs [74]. In previous studies, the role of DMRT1 in maintaining SC differentiation was demonstrated through conditional deletion of *Dmrt1* in SCs [42]. Without DMRT1, SCs lost expression of SOX9, a male-specific transcription factor, and gained expression of FOXL2, a female-specific

transcription factor, indicating that DMRT1 is needed to maintain the male-specific program and inhibit the female-specific program. In the current study, characterization of *Dmrt1*$^{-/-}$ and *Dmrt1*$^{-/-;tg}$ mice identified additional roles of DMRT1 in SC differentiation. This included a role in nuclear maturation, as seen by differences in SC nuclear morphology and size between wild-type and *Dmrt1*$^{-/-}$ and *Dmrt1*$^{-/-;tg}$ mice [67, 68]. In *Dmrt1*$^{-/-}$ and *Dmrt1*$^{-/-;tg}$ mice, the normal postpubertal nuclear transition was significantly altered. Thus, at P42, nuclei in *Dmrt1*$^{-/-}$ SCs retained their prepubertal appearance and size, while those in *Dmrt1*$^{-/-;tg}$ SCs appeared to have partially transitioned to the postpubertal state observed in wild-type mice (Fig. 5). The findings indicate that DMRT1 regulates SC nuclear maturation both by autonomous actions in SCs and by nonautonomous effects on either GC function and/or survival.

Gene expression analyses also supported DMRT1's role in SC maturation, confirming previous findings on *Gata1* and *Ar*, genes associated with mature SCs, and identifying *Krt18*, a marker of immature SCs, as a DMRT1-regulated gene [2, 60, 61, 74–79]. In both *Dmrt1*$^{-/-}$ and *Dmrt1*$^{-/-;tg}$ testes, *Gata1* transcript levels decreased, while those for *Krt18* increased (Fig. 4). Notably, for both genes, return of DMRT1 to SCs did not correct the altered expression, indicating that their proper expression requires *Dmrt1* in GCs. Previous studies showed that GATA1 expression was significantly decreased in P14 testes containing an SC conditional deletion of *Dmrt1* (*SCDmrt1KO*), which, together with the current data, indicates that DMRT1 is needed in both SCs and GCs (indirectly) for *Gata1* expression [2]. Furthermore, previous studies showed that GC deficiency (from various mutant models) or deletion of *Dmrt1* in the GCs (*GCDmrt1KO*) eliminated the normal cyclic expression pattern of GATA1 in SCs [5, 61]. The earlier GC deficiency study also concluded that differentiating GCs negatively regulated GATA1 [61]. Together with our study, which indicates that *Gata1* expression is positively regulated by undifferentiated GC under DMRT1's influence, the findings suggest that stage-specific expression of GATA1 results from the combination of positive and negative regulation imparted by undifferentiated and differentiated GCs, respectively [61].

Expression of *Ar*, a gene associated with SC maturation, was examined by RT-PCR (P7) and immunohistochemistry (P7 and P15). At P7, *Ar*/AR expression was similar between genotypes (Fig. 4 and Supplemental Figure S4). However, by P15, immunohistochemistry revealed a notable reduction in AR-positive SCs in *Dmrt1*$^{-/-}$ testes, which was markedly improved by the presence of the transgene, indicating that DMRT1 in SCs is needed, after P7, to induce AR expression in SCs (Fig. 4 and Supplemental Figure S4). The findings are consistent with a previous report showing that the induction of AR in SCs, which occurred between P5 and P9 in wild-type mice, was absent in *SCDmrt1KO* mice [2]. Thus, in addition to substantiating the importance of DMRT1 to proper AR expression, the consistency between reports supports use of the transgenic model as an alternative approach to determine DMRT1 function.

Evaluation of the transgenic mice on a wild-type background revealed another important role for DMRT1 in SCs. In particular, the studies showed that the *Wt1-Dmrt1* transgene protected against the normal age-related declined in testis weight. Thus, at 18 mo, testis weights of wild-type mice were reduced by 50%, compared to the weight of 3-mo-old mice, while testis weights of the transgenic mice were reduced by only 25%. Since testis weight is a strong indicator of spermatogenic capacity, the additional DMRT1, directed by the transgene, appears to have maintained SC functions that normally support spermatogenesis and diminish with age. Interestingly, the presence of the transgene also had a protective effect on sperm progressive motility. Thus, similar to that observed in aging men, there was a dramatic age-dependent decrease in mouse sperm progressive motility, which was less severe in the presence of the transgene (Fig. 3D [80–82]).

The findings are consistent with the idea that additional DMRT1 improves the overall capacity of SCs to nurture the developing GCs, thereby preserving both spermatogenic capacity and sperm function. It also suggests that, in older animals, there is a normal age-related decline in DMRT1 activity that was, in part, rescued by additional DMRT1 from the transgene. Alternatively, it suggests that DMRT1 from the transgene helped to prevent a decline in SC function directed by another mechanism. While an age-dependent decrease in SC DMRT1 could explain one of the possibilities, accurate assessment was problematic. In particular, immunohistochemistry failed to detect any major differences between wild-type and transgenic mice in DMRT1 levels in SCs (data not shown), and it is not accurate enough to assess moderate expression changes. Western blot evaluation of isolated SC proteins was not attempted because DMRT1 levels drops dramatically in cultured cells, and therefore the assay would inappropriately favor the transgenic cells. Therefore, the mechanism associated with DMRT1's protective role remains uncertain.

Studies with *Dmrt1*$^{-/-}$ and *Dmrt1*$^{-/-;tg}$ male mice also revealed roles for DMRT1 in establishing and/or maintaining seminiferous tubule integrity and polarity. At P7, seminiferous tubule morphology was similar between genotypes. However, at P42, tubule structures were barely discernible in *Dmrt1*$^{-/-}$ mice, while they were clearly evident in *Dmrt1*$^{-/-;tg}$ mice (Fig. 6). This confirmed previous results in *SCDmrt1KO* mice that showed normal tubule integrity at P7 and disorganized tubules without defined lumens at P28 [2, 24]. While there was some variability in tubule structure between samples, due to either sample preparation or differences between transgenic lines, complete restoration of seminiferous tubule morphology was consistent in line 37 *Dmrt1*$^{-/-;tg}$ animals, which showed the strongest DMRT1 expression. The apparent regulation of *Espin* mRNA by DMRT1 in SCs (Fig. 4) prompted further examination of the seminiferous epithelium for the presence and localization of ES, testis-specific adherens junctions [64]. ES are unique actin-containing structures that form at distinct apical and basal sites of intercellular attachment in SCs [83]. Apical ES are located at the interface between SCs and spermatids and are required not only for attaching the cells but also for spermatid translocation and timing the release of spermatozoa. Basal ES form at the interface between SCs at the site of the blood-testis barrier. To determine if DMRT1 affects the formation of these junctions, expression of ES-associated proteins ESPIN and NECTIN-2 was evaluated. ESPIN, an ACTIN-binding protein, and NECTIN-2, a member of the Ig superfamily that mediates cell-cell adhesion, localize to both basal and apical ES in SCs [84–86]. In complete absence of DMRT1, these two proteins were significantly reduced in P42 testes and showed no specific organization or location (Figs. 7 and 8). In contrast, in *Dmrt1*$^{-/-;tg}$ testes, with DMRT1 expressed only in SCs, ESPIN and NECTIN-2 regained their expression and localized, together with ACTIN, in the apical region of the tubule but not the basal region, despite the presence of ACTIN. Given that previous findings indicated that NECTIN-2 is required for ES formation and showed, in its absence, that ESPIN failed to localize to the apical ES, it is likely that the observed changes in ESPIN resulted from changes in NECTIN-2 [85]. Interesting, the apical-only

location resembled that of tight junction protein 1 (Tjp1, aka ZO-1), as seen in immature mouse testes prior to tight junction formation, and for ESPIN in P10 and hypogonadal mouse testes [87, 88]. Furthermore, both current and past studies demonstrated diminished expression of several tight junction proteins (Fig. 7 [20]), suggesting that ESPIN and NECTIN-2 failed to locate basally because tight junctions are absent or defective and consequently that DMRT1 is needed in the GCs for tight junction formation. Together, these findings indicate that DMRT1 in SCs directs expression and apical location of ESPIN and NECTIN-2, while their basal location also requires DMRT1 in GCs to assemble tight junctions, which are needed for basal location of the ES.

In summary, the histological and gene expression results show that the *Dmrt1*$^{-/-;tg}$ mice uphold several key requirements that support their use to delineate DMRT1 function and identify the cell-specific effects of DMRT1. In particular, transgenic DMRT1 was produced only in testicular SCs, recapitulated several previously identified DMRT1 functions, and revealed new features of DMRT1 with respect to its role in the germ line and SC maturation and integrity. Unlike existing GC-specific deletion models, GC deficiency in *Dmrt1*$^{-/-;tg}$ mice is free from temporal and expression constraints of a *Cre* transgene [2, 3, 5]. Notably, an important difference between the *Dmrt1*$^{-/-;tg}$ model and those generated by *Tnap-Cre* and *Ngn3-Cre* is its ability to effectively profile early events in postnatal testis development, such as those needed to establish the stem cell population and the first wave of spermatogenesis. Note, that, in addition to *Tnap-Cre* and *Ngn3-Cre*, *Nanos3*-Cre was used to delete *Dmrt1* from GCs, but little information is available on the transgenes efficacy or the phenotype following *Dmrt1* deletion [42].Therefore, *Dmrt1*$^{-/-;tg}$ mice nicely complement existing models of DMRT1 deficiency, and their continued evaluation will provide new insight into DMRT1 function.

ACKNOWLEDGMENT

We thank members of the Heckert lab for many helpful discussions and Dr. Gustavo Blanco and his laboratory for their assistance with sperm functional analysis.

REFERENCES

1. Ferguson-Smith M. The evolution of sex chromosomes and sex determination in vertebrates and the key role of DMRT1. Sex Dev 2007; 1:2–11.
2. Kim S, Bardwell VJ, Zarkower D. Cell type-autonomous and non-autonomous requirements for Dmrt1 in postnatal testis differentiation. Dev Biol 2007; 307:314–327.
3. Krentz AD, Murphy MW, Kim S, Cook MS, Capel B, Zhu R, Matin A, Sarver AL, Parker KL, Griswold MD, Looijenga LH, Bardwell VJ, et al. The DM domain protein DMRT1 is a dose-sensitive regulator of fetal germ cell proliferation and pluripotency. Proc Natl Acad Sci U S A 2009; 106:22323–22328.
4. Marchand O, Govoroun M, D'Cotta H, McMeel O, Lareyre J, Bernot A, Laudet V, Guiguen Y. DMRT1 expression during gonadal differentiation and spermatogenesis in the rainbow trout, *Oncorhynchus mykiss*. Biochim Biophys Acta 2000; 1493:180–187.
5. Matson CK, Murphy MW, Griswold MD, Yoshida S, Bardwell VJ, Zarkower D. The mammalian doublesex homolog DMRT1 is a transcriptional gatekeeper that controls the mitosis versus meiosis decision in male germ cells. Dev Cell 2010; 19:612–624.
6. Erdman SE, Burtis KC. The Drosophila doublesex proteins share a novel zinc finger related DNA binding domain. EMBO J 1993; 12:527–535.
7. Raymond CS, Shamu CE, Shen MM, Seifert KJ, Hirsch B, Hodgkin J, Zarkower D. Evidence for evolutionary conservation of sex-determining genes. Nature 1998; 391:691–695.
8. Zhu L, Wilken J, Phillips NB, Narendra U, Chan G, Stratton SM, Kent SB, Weiss MA. Sexual dimorphism in diverse metazoans is regulated by a novel class of intertwined zinc fingers. Genes Dev 2000; 14:1750–1764.
9. Volff JN, Zarkower D, Bardwell VJ, Schartl M. Evolutionary dynamics of the DM domain gene family in metazoans. J Mol Evol 2003; 57(suppl 1): S241–S249.
10. Bratus A, Slota E. DMRT1/Dmrt1, the sex determining or sex differentiating gene in Vertebrata. Folia Biol (Krakow) 2006; 54:81–86.
11. Nagahama Y. Molecular mechanisms of sex determination and gonadal sex differentiation in fish. Fish Physiol Biochem 2005; 31:105–109.
12. Smith CA, Sinclair AH. Sex determination: insights from the chicken. Bioessays 2004; 26:120–132.
13. Sinclair A, Smith C, Western P, McClive P. A comparative analysis of vertebrate sex determination. Novartis Found Symp 2002; 244:102–111; discussion 111–104, 203–106, 253–107.
14. Smith CA, McClive PJ, Western PS, Reed KJ, Sinclair AH. Conservation of a sex-determining gene. Nature 1999; 402:601–602.
15. Boyer A, Dornan S, Daneau I, Lussier J, Silversides DW. Conservation of the function of DMRT1 regulatory sequences in mammalian sex differentiation. Genesis 2002; 34:236–243.
16. Hong CS, Park BY, Saint-Jeannet JP. The function of Dmrt genes in vertebrate development: it is not just about sex. Dev Biol 2007; 310:1–9.
17. Lints R, Emmons SW. Regulation of sex-specific differentiation and mating behavior in *C. elegans* by a new member of the DM domain transcription factor family. Genes Dev 2002; 16:2390–2402.
18. Zhang W, Li B, Singh R, Narendra U, Zhu L, Weiss MA. Regulation of sexual dimorphism: mutational and chemogenetic analysis of the double-sex DM domain. Mol Cell Biol 2006; 26:535–547.
19. Raymond CS, Kettlewell JR, Hirsch B, Bardwell VJ, Zarkower D. Expression of Dmrt1 in the genital ridge of mouse and chicken embryos suggests a role in vertebrate sexual development. Dev Biol 1999; 215: 208–220.
20. Fahrioglu U, Murphy MW, Zarkower D, Bardwell VJ. mRNA expression analysis and the molecular basis of neonatal testis defects in Dmrt1 mutant mice. Sex Dev 2007; 1:42–58.
21. Herpin A, Schartl M. Molecular mechanisms of sex determination and evolution of the Y-chromosome: insights from the medakafish (*Oryzias latipes*). Mol Cell Endocrinol 2009; 306:51–58.
22. Koopman P. The delicate balance between male and female sex determining pathways: potential for disruption of early steps in sexual development. Int J Androl 2010; 33:252–258.
23. Moniot B, Berta P, Scherer G, Sudbeck P, Poulat F. Male specific expression suggests role of DMRT1 in human sex determination. Mech Dev 2000; 91:323–325.
24. Raymond CS, Murphy MW, O'Sullivan MG, Bardwell VJ, Zarkower D. Dmrt1, a gene related to worm and fly sexual regulators, is required for mammalian testis differentiation. Genes Dev 2000; 14:2587–2595.
25. Rhen T, Schroeder A. Molecular mechanisms of sex determination in reptiles. Sex Dev 2010; 4:16–28.
26. Smith CA, Roeszler KN, Ohnesorg T, Cummins DM, Farlie PG, Doran TJ, Sinclair AH. The avian Z-linked gene DMRT1 is required for male sex determination in the chicken. Nature 2009; 461:267–271.
27. Lei N, Hornbaker KI, Rice DA, Karpova T, Agbor VA, Heckert LL. Sex-specific differences in mouse DMRT1 expression are both cell type- and stage-dependent during gonad development. Biol Reprod 2007; 77: 466–475.
28. Kettlewell JR, Raymond CS, Zarkower D. Temperature-dependent expression of turtle Dmrt1 prior to sexual differentiation. Genesis 2000; 26:174–178.
29. Repetto GM, Wagstaff J, Korf BR, Knoll JH. Complex familial rearrangement of chromosome 9p24.3 detected by FISH. Am J Med Genet 1998; 76:306–309.
30. Christ LA, Crowe CA, Micale MA, Conroy JM, Schwartz S. Chromosome breakage hotspots and delineation of the critical region for the 9p-deletion syndrome. Am J Hum Genet 1999; 65:1387–1395.
31. Swinkels ME, Simons A, Smeets DF, Vissers LE, Veltman JA, Pfundt R, de Vries BB, Faas BH, Schrander-Stumpel CT, McCann E, Sweeney E, May P, et al. Clinical and cytogenetic characterization of 13 Dutch patients with deletion 9p syndrome: delineation of the critical region for a consensus phenotype. Am J Med Genet A 2008; 146A:1430–1438.
32. Barbaro M, Balsamo A, Anderlid BM, Myhre AG, Gennari M, Nicoletti A, Pittalis MC, Oscarson M, Wedell A. Characterization of deletions at 9p affecting the candidate regions for sex reversal and deletion 9p syndrome by MLPA. Eur J Hum Genet 2009; 17:1439–1447.
33. Vinci G, Chantot-Bastaraud S, El Houate B, Lortat-Jacob S, Brauner R, McElreavey K. Association of deletion 9p, 46, XY gonadal dysgenesis and autistic spectrum disorder. Mol Hum Reprod 2007; 13:685–689.
34. Vasquez-Velasquez AI, Arnaud-Lopez L, Figuera LE, Padilla-Gutierrez JR, Rivas F, Rivera H. Ambiguous genitalia by 9p deletion inherent to a dic(Y;9)(q12;p24). J Appl Genet 2005; 46:415–418.

35. Ounap K, Uibo O, Zordania R, Kiho L, Ilus T, Oiglane-Shlik E, Bartsch O. Three patients with 9p deletions including DMRT1 and DMRT2: a girl with XY complement, bilateral ovotestes, and extreme growth retardation, and two XX females with normal pubertal development. Am J Med Genet A 2004; 130A:415–423.
36. Vialard F, Ottolenghi C, Gonzales M, Choiset A, Girard S, Siffroi JP, McElreavey K, Vibert-Guigue C, Sebaoun M, Joye N, Portnoi MF, Jaubert F, et al. Deletion of 9p associated with gonadal dysfunction in 46, XY but not in 46, XX human fetuses. J Med Genet 2002; 39:514–518.
37. Shetty S, Kirby P, Zarkower D, Graves JA. DMRT1 in a ratite bird: evidence for a role in sex determination and discovery of a putative regulatory element. Cytogenet Genome Res 2002; 99:245–251.
38. Yi W, Zarkower D. Similarity of DNA binding and transcriptional regulation by *Caenorhabditis elegans* MAB-3 and *Drosophila melanogaster* DSX suggests conservation of sex determining mechanisms. Development 1999; 126:873–881.
39. Herpin A, Schartl M. Dmrt1 genes at the crossroads: a widespread and central class of sexual development factors in fish. FEBS J 2011; 278: 1010–1019.
40. Koopman P. Sex determination: the power of DMRT1. Trends Genet 2009; 25:479–481.
41. Krentz AD, Murphy MW, Sarver AL, Griswold MD, Bardwell VJ, Zarkower D. DMRT1 promotes oogenesis by transcriptional activation of Stra8 in the mammalian fetal ovary. Dev Biol 2011; 356:63–70.
42. Matson CK, Murphy MW, Sarver AL, Griswold MD, Bardwell VJ, Zarkower D. DMRT1 prevents female reprogramming in the postnatal mammalian testis. Nature 2011; 476:101–104.
43. Yoshida S, Sukeno M, Nakagawa T, Ohbo K, Nagamatsu G, Suda T, Nabeshima Y. The first round of mouse spermatogenesis is a distinctive program that lacks the self-renewing spermatogonia stage. Development 2006; 133:1495–1505.
44. Yoshida S, Takakura A, Ohbo K, Abe K, Wakabayashi J, Yamamoto M, Suda T, Nabeshima Y. Neurogenin3 delineates the earliest stages of spermatogenesis in the mouse testis. Dev Biol 2004; 269:447–458.
45. Karpova T, Presley J, Manimaran RR, Scherrer SP, Tejada L, Peterson KR, Heckert LL. A FTZ-F1-containing yeast artificial chromosome recapitulates expression of steroidogenic factor 1 in vivo. Mol Endocrinol 2005; 19:2549–2563.
46. Godwin AR, Capecchi MR. Hoxc13 mutant mice lack external hair. Genes Dev 1998; 12:11–20.
47. Poorkaj P, Peterson KR, Schellenberg GD. Single-step conversion of P1 and P1 artificial chromosome clones into yeast artificial chromosomes. Genomics 2000; 68:106–110.
48. Burgers PM, Percival KJ. Transformation of yeast spheroplasts without cell fusion. Anal Biochem 1987; 163:391–397.
49. Hermann BP, Hornbaker KI, Maran RR, Heckert LL. Distal regulatory elements are required for Fshr expression, in vivo. Mol Cell Endocrinol 2007; 260–262:49–58.
50. Karpova T, Maran RR, Presley J, Scherrer SP, Tejada L, Heckert LL. Transgenic rescue of SF-1-null mice. Ann N Y Acad Sci 2005; 1061: 55–64.
51. Peterson KR, Clegg CH, Li Q, Stamatoyannopoulos G. Production of transgenic mice with yeast artificial chromosomes. Trends Genet 1997; 13: 61–66.
52. Peterson KR. Production and analysis of transgenic mice containing yeast artificial chromosomes. Genet Eng (N Y) 1997; 19:235–255.
53. Jimenez T, Sanchez G, Wertheimer E, Blanco G. Activity of the Na, K-ATPase alpha4 isoform is important for membrane potential, intracellular Ca2+, and pH to maintain motility in rat spermatozoa. Reproduction 2010; 139:835–845.
54. Schneider CA, Rasband WS, Eliceiri KW. NIH Image to ImageJ: 25 years of image analysis. Nat Methods 2012; 9:671–675.
55. Heckert LL, Sawadogo M, Daggett MA, Chen JK. The USF proteins regulate transcription of the follicle-stimulating hormone receptor but are insufficient for cell-specific expression. Mol Endocrinol 2000; 14: 1836–1848.
56. Gifford CA, Racicot K, Clark DS, Austin KJ, Hansen TR, Lucy MC, Davies CJ, Ott TL. Regulation of interferon-stimulated genes in peripheral blood leukocytes in pregnant and bred, nonpregnant dairy cows. J Dairy Sci 2007; 90:274–280.
57. Livak KJ, Schmittgen TD. Analysis of relative gene expression data using real-time quantitative PCR and the 2(-Delta Delta C(T)) method. Methods 2001; 25:402–408.
58. Vidal VP, Chaboissier MC, de Rooij DG, Schedl A. Sox9 induces testis development in XX transgenic mice. Nat Genet 2001; 28:216–217.
59. Moore AW, Schedl A, McInnes L, Doyle M, Hecksher-Sorensen J, Hastie ND. YAC transgenic analysis reveals Wilms' tumour 1 gene activity in the proliferating coelomic epithelium, developing diaphragm and limb. Mech Dev 1998; 79:169–184.
60. Tarulli GA, Stanton PG, Lerchl A, Meachem SJ. Adult Sertoli cells are not terminally differentiated in the Djungarian hamster: effect of FSH on proliferation and junction protein organization. Biol Reprod 2006; 74: 798–806.
61. Yomogida K, Ohtani H, Harigae H, Ito E, Nishimune Y, Engel JD, Yamamoto M. Developmental stage- and spermatogenic cycle-specific expression of transcription factor GATA-1 in mouse Sertoli cells. Development 1994; 120:1759–1766.
62. Imai T, Kawai Y, Tadokoro Y, Yamamoto M, Nishimune Y, Yomogida K. In vivo and in vitro constant expression of GATA-4 in mouse postnatal Sertoli cells. Mol Cell Endocrinol 2004; 214:107–115.
63. Russell LD, Bartke A, Goh JC. Postnatal development of the Sertoli cell barrier, tubular lumen, and cytoskeleton of Sertoli and myoid cells in the rat, and their relationship to tubular fluid secretion and flow. Am J Anat 1989; 184:179–189.
64. Cheng CY, Mruk DD. Regulation of spermiogenesis, spermiation and blood-testis barrier dynamics: novel insights from studies on Eps8 and Arp3. Biochem J 2011; 435:553–562.
65. Cheng CY, Mruk DD. Cell junction dynamics in the testis: Sertoli-germ cell interactions and male contraceptive development. Physiol Rev 2002; 82:825–874.
66. Mruk DD, Cheng CY. Tight junctions in the testis: new perspectives. Philos Trans R Soc Lond B Biol Sci 2010; 365:1621–1635.
67. Ramos AS Jr, Dym M. Ultrastructural differentiation of rat Sertoli cells. Biol Reprod 1979; 21:909–922.
68. Russell LD, Ren HP, Sinha Hikim I, Schulze W, Sinha Hikim AP. A comparative study in twelve mammalian species of volume densities, volumes, and numerical densities of selected testis components, emphasizing those related to the Sertoli cell. Am J Anat 1990; 188:21–30.
69. Nagano R, Tabata S, Nakanishi Y, Ohsako S, Kurohmaru M, Hayashi Y. Reproliferation and relocation of mouse male germ cells (gonocytes) during prespermatogenesis. Anat Rec 2000; 258:210–220.
70. Montoliu L. Gene transfer strategies in animal transgenesis. Cloning Stem Cells 2002; 4:39–46.
71. Pelletier J, Schalling M, Buckler AJ, Rogers A, Haber DA, Housman D. Expression of the Wilms' tumor gene WT1 in the murine urogenital system. Genes Dev 1991; 5:1345–1356.
72. Mundlos S, Pelletier J, Darveau A, Bachmann M, Winterpacht A, Zabel B. Nuclear localization of the protein encoded by the Wilms' tumor gene WT1 in embryonic and adult tissues. Development 1993; 119:1329–1341.
73. Buckler AJ, Pelletier J, Haber DA, Glaser T, Housman DE. Isolation, characterization, and expression of the murine Wilms' tumor gene (WT1) during kidney development. Mol Cell Biol 1991; 11:1707–1712.
74. Sharpe RM, McKinnell C, Kivlin C, Fisher JS. Proliferation and functional maturation of Sertoli cells, and their relevance to disorders of testis function in adulthood. Reproduction 2003; 125:769–784.
75. Armstrong JF, Pritchard-Jones K, Bickmore WA, Hastie ND, Bard JB. The expression of the Wilms' tumour gene, WT1, in the developing mammalian embryo. Mech Dev 1993; 40:85–97.
76. Ketola I, Anttonen M, Vaskivuo T, Tapanainen JS, Toppari J, Heikinheimo M. Developmental expression and spermatogenic stage specificity of transcription factors GATA-1 and GATA-4 and their cofactors FOG-1 and FOG-2 in the mouse testis. Eur J Endocrinol 2002; 147:397–406.
77. LaVoie HA. The role of GATA in mammalian reproduction. Exp Biol Med (Maywood) 2003; 228:1282–1290.
78. Maga G, Hubscher U. Proliferating cell nuclear antigen (PCNA): a dancer with many partners. J Cell Sci 2003; 116:3051–3060.
79. Bar-Shira Maymon B, Paz G, Elliott DJ, Hammel I, Kleiman SE, Yogev L, Hauser R, Botchan A, Yavetz H. Maturation phenotype of Sertoli cells in testicular biopsies of azoospermic men. Hum Reprod 2000; 15: 1537–1542.
80. Jung A, Schuppe HC, Schill WB. Comparison of semen quality in older and younger men attending an andrology clinic. Andrologia 2002; 34: 116–122.
81. Eskenazi B, Wyrobek AJ, Sloter E, Kidd SA, Moore L, Young S, Moore D. The association of age and semen quality in healthy men. Hum Reprod 2003; 18:447–454.
82. Levitas E, Lunenfeld E, Weisz N, Friger M, Potashnik G. Relationship between age and semen parameters in men with normal sperm concentration: analysis of 6022 semen samples. Andrologia 2007; 39: 45–50.
83. Vogl AW, Pfeiffer DC, Redenbach DM. Ectoplasmic (''junctional'') specializations in mammalian Sertoli cells: influence on spermatogenic cells. Ann N Y Acad Sci 1991; 637:175–202.

84. Bartles JR, Wierda A, Zheng L. Identification and characterization of espin, an actin-binding protein localized to the F-actin-rich junctional plaques of Sertoli cell ectoplasmic specializations. J Cell Sci 1996; 109(pt 6):1229–1239.
85. Mueller S, Rosenquist TA, Takai Y, Bronson RA, Wimmer E. Loss of nectin-2 at Sertoli-spermatid junctions leads to male infertility and correlates with severe spermatozoan head and midpiece malformation, impaired binding to the zona pellucida, and oocyte penetration. Biol Reprod 2003; 69:1330–1340.
86. Ozaki-Kuroda K, Nakanishi H, Ohta H, Tanaka H, Kurihara H, Mueller S, Irie K, Ikeda W, Sakai T, Wimmer E, Nishimune Y, Takai Y. Nectin couples cell-cell adhesion and the actin scaffold at heterotypic testicular junctions. Curr Biol 2002; 12:1145–1150.
87. Byers S, Graham R, Dai HN, Hoxter B. Development of Sertoli cell junctional specializations and the distribution of the tight-junction-associated protein ZO-1 in the mouse testis. Am J Anat 1991; 191:35–47.
88. Myers M, Ebling FJ, Nwagwu M, Boulton R, Wadhwa K, Stewart J, Kerr JB. Atypical development of Sertoli cells and impairment of spermatogenesis in the hypogonadal (hpg) mouse. J Anat 2005; 207:797–811.